Phenotypic plasticity in bacterial elongation among closely related species

Marie Delaby[1,#], Liu Yang[1,2,#], Maxime Jacq[1], Kelley A Gallagher[1,3], David T Kysela[1], Velocity Hughes[1,4], Francisco Pulido[5], Frederic J. Veyrier[5], Michael S. VanNieuwenhze[6], Yves V. Brun[1,7*]

[1]Département de microbiologie, infectiologie et immunologie, Université de Montréal, C.P. 6128, succ. Centre-ville, Montréal (Québec) H3C 3J7, Canada

[2]Current Address: Biosphere Sciences and Engineering, Carnegie Institution of Washington, 813 Santa Barbara Street, Pasadena, California, 91101, United States

[3]Current address: Department of Microbiology, Cornell University, Ithaca, NY, USA

[4]Synthesis by Velocity, Malmö, Sweden

[5]Bacterial Symbionts Evolution, Centre Armand-Frappier Santé Biotechnologie, Institut National de la Recherche Scientifique, Laval, QC, H7V 1B7, Canada

[6]Department of Chemistry, Indiana University, 800 East Kirkwood Avenue, Bloomington, IN 47405, USA

[7]Department of Biology, Indiana University, 1001 E. 3rd St, Bloomington, IN 47405, USA

# contributed equally

*Address correspondence to Yves V. Brun, yves.brun@umontreal.ca

Keywords : Elongation modes, midcell elongation, Peptidoglycan, Caulobacteraceae, Caulobacter

ABSTRACT

Cell elongation is a fundamental component of the bacterial cell cycle and has been studied over many decades, in part owing to its mechanisms being a target of numerous antibiotic classes. While several distinct modes of cell elongation have been described, these studies have largely relied on a handful of model bacterial species. Therefore, we have a limited view of the diversity of cell elongation approaches that are employed by bacteria, and how these vary in response to evolutionary and environmental influences. Here, by employing fluorescent D-amino acids (FDAAs) to track the spatiotemporal dynamics of elongation, we reveal previously unsuspected diversity of elongation modes among closely related species of the *Caulobacteraceae*, with species-specific combinations of dispersed, midcell and polar elongation that can be either unidirectional or bidirectional. Using genetic, cell biology, and phylogenetic approaches, we demonstrate that evolution of unidirectional-midcell elongation is accompanied by changes in the localization pattern of the peptidoglycan synthase PBP2 and infer that elongation complexes display a high degree of phenotypic plasticity, both among the *Caulobacteraceae* and more widely among the Alphaproteobacteria. Demonstration that even closely related bacterial species employ highly distinct mechanisms of cell elongation reshapes our understanding of the evolution and regulation of bacterial cell growth, with broad implications for bacterial morphology, adaptation, and antibiotic resistance.

INTRODUCTION

Cell elongation is a fundamental process in bacteria, underlying cell growth, morphogenesis and division. Mechanisms of cell elongation are strictly regulated but respond dynamically to developmental and environmental cues[1-3]. For instance, spatiotemporal patterns of cell elongation are modulated over the cell cycle in many bacterial species. In others, nutrient starvation can trigger specialized modes of elongation, resulting in shape changes to improve nutrient uptake. Over the course of evolution, mechanisms of cell elongation have also diversified, as evidenced by the variety of cell shapes, life cycles and mechanisms of growth seen in bacteria[4,5].

At the structural level, bacterial cell elongation is driven by the synthesis of the peptidoglycan (PG) cell wall, a meshwork of glycan strands crosslinked by peptide chains that confers structural integrity to the cell[3,6,7]. Synthesis of PG is essential to bacterial growth and division[8] and is catalyzed by the penicillin binding proteins (PBPs) acting in concert with regulatory protein complexes called the elongasome (for cell elongation) and the divisome (for cell division). Although the PBPs, the elongasome and the divisome are widely conserved among bacteria, different species have been shown to employ distinct sets of proteins to assemble their elongasomes[9-14]. Such modularity and flexibility in the regulation of cell elongation at the molecular level may underlie the evolution and diversification of bacterial cell elongation mechanisms. Indeed, recent studies have found that disparate mechanisms of cell elongation can yield similar shapes: a rod-shaped cell can be generated by a dispersed, a lateral elongation mode, or by zonal elongation from one or both cell poles or the midcell (**Fig. 1a**)[9,15-19]. Conversely, the same elongation mode can generate different cell shapes: spherical, ovoid, rod, and crescent shapes can be generated by bidirectional elongation from the midcell[20,21]. However, our understanding of the diversity of elongation modes in bacteria is primarily based on a few distantly related model

organisms, leading to the assumption that closely related species share the same elongation strategies. Consequently, the true diversity of bacterial cell elongation mechanisms may be greatly underappreciated, and our insights reveal little about the evolutionary mechanisms driving these differences.

To address this knowledge gap, our study explores how distinct elongation modes evolved within closely related, morphologically diverse bacterial species from the *Caulobacteraceae* family[4,5,22]. Within this family, the well-studied model organism *Caulobacter crescentus* uses bidirectional elongation from the midcell[23] (**Fig. 1b**). By studying its related species, we discover two novel elongation modes – unidirectional midcell elongation in the species *Asticcacaulis excentricus*, and polar plus unidirectional midcell elongation *in Asticcacaulis biprosthecum*. Using a multidisciplinary approach that integrates live-cell imaging with genetic and evolutionary analysis, we explore these elongation mechanisms. Our findings reveal that the evolution of these elongation strategies is associated with shifts in the spatial localization of a core elongasome enzyme. Specifically, we show that the penicillin binding protein PBP2, which localizes diffusely in *C. crescentus*, concentrates at the midcell in *A. excentricus,* where it serves as the transpeptidase enzyme driving unidirectional PG synthesis. This highlights how the regulation of conserved elongasome machinery can vary even between closely related species, potentially aligning with broader evolutionary pressures. Extending our analysis beyond the *Caulobacteraceae*, we found that *Rhodobacter capsulatus* shares the unidirectional midcell elongation pattern seen in *A. excentricus*, and we further infer from the phylogeny of the Alphaproteobacteria that bacterial cell elongation mechanisms display far greater phenotypic plasticity than previously anticipated. Ultimately, these results challenge the notion that closely related species share the same elongation

mode. Instead, they reveal an unexplored diversity in elongation mechanisms, as cells respond to evolutionary forces to generate diversity in growth modes even at close evolutionary scales.

RESULTS

C. crescentus and *A. excentricus* have different patterns of PG synthesis

The order *Caulobacterales* exhibits at least three elongation modes – dispersed, polar and midcell[4], suggesting that it could be a good model for studying the evolution of cell elongation. The order comprises three families: the *Caulobacteraceae*, the *Hyphomonadaceae*, and the *Maricaulaceae*. The *Hyphomonadaceae* elongate polarly through budding[24-26], but the elongation modes in the *Maricaulaceae* and the *Caulobacteraceae* are unknown, with the exception of the model organism *C. crescentus,* which predominantly grows through bidirectional midcell elongation, with some dispersed elongation during early stages of the cell cycle (**Fig. 1b**).

To determine the elongation modes in other *Caulobacteraceae*, we analyzed the genus *Asticcacaulis,* comparing *C. crescentus* and *A. excentricus* using pulse-chase experiments with fluorescent D-amino acids (FDAAs). FDAAs are fluorescent dyes that are incorporated into the PG by PG transpeptidases, serving as highly effective tools to observe the dynamics of cell growth in various colors (in this study, we use the dyes BADA, HADA and TADA, see Methods)[27,28]. To track PG synthesis/turnover in real-time relative to the cell division site, we marked the division site in *C. crescentus* using ZapA-mCherry and in *A. excentricus* using ZapA-sfGFP[29], and performed pulse-chase experiments using FDAAs with complementary fluorophores. Briefly, we labeled whole-cell PG with FDAA (the "pulse") over two generations, washed the cells to remove free FDAA, and observed the cells during a period of growth in the absence of FDAA (the "chase") by time-lapse microscopy (**Fig. 1c**). During the chase period, the loss of FDAA labeling reveals spatial patterns of new PG incorporation[30].

In dimorphic bacteria such as *Asticcacaulis* and *Caulobacter* species, the new pole generated by division gives rise to a motile swarmer cell, while the old pole forms the larger, non-

motile stalked cell, reflecting the species' characteristic asymmetric division. In *C. crescentus*, visualizing the retention and loss of the FDAA label throughout the cell cycle, we observed that the loss of FDAA labeling occurred from the division plane defined by ZapA-mCherry, and extended bidirectionally towards both cell poles (**Fig. 1d and Extended Data Fig. 1a)**. Conversely, in *A. excentricus*, the loss of FDAA labeling originated from the division plane but moved predominantly towards the new pole of the dividing cell (**Fig. 1d and Extended Data Fig. 1b)**. Later in the cell cycle, *A. excentricus* cells also began losing FDAA signal on the old pole side of the ZapA-sfGFP signal once constriction was initiated (**Fig. 1d, white stars**). This loss of FDAA signal on the old pole side of the division plane during constriction likely corresponds to PG synthesis during septation and cell division. Together, these data indicate that PG synthesis/turnover for cell elongation are spatially localized close to the future site of cell division in both *C. crescentus* and *A. excentricus*. Furthermore, they indicate a variation in PG synthesis/turnover dynamics in these two closely related species, in which *C. crescentus* elongates bidirectionally and *A. excentricus* towards the new pole (**Fig. 1b and 1e**).

A. excentricus **elongates unidirectionally from the midcell towards the new pole**

To further investigate the position and directionality of PG synthesis during midcell elongation in *A. excentricus*, we conducted sequential short-pulse FDAA labeling experiments with differently colored FDAAs. This approach allows us to track active sites of PG synthesis in growing cells based on the spatial pattern of incorporation of the sequentially applied dyes over time[30]. If the signal from the first FDAA (red) pulse appears on both sides of the second FDAA (green), PG incorporation can be inferred to occur bidirectionally, whereas if the first FDAA signal appears on one side of the second signal, it would indicate unidirectional elongation (**Fig. 2a**).

For these experiments, *A. excentricus* and *C. crescentus* cells were first grown in the presence of one FDAA (shown in red) for 5% of their generation time, washed to remove excess dye, and then subjected to a second pulse with a different FDAA (shown in green) (**Fig. 2a**). In *C. crescentus*, the first, red FDAA signal appeared on both sides of the second, green signal, which was approximately located at the midcell (**Fig. 2b)**. To analyse these patterns quantitatively, we generated demographs, which are graphical summaries of fluorescence intensities, where cells are sorted by length along the y-axis, and aligned at the center by their midcell as a proxy for cell cycle progression. Demograph analysis of *C. crescentus* cells confirmed that their first FDAA signal was located on both sides of the second signal in all but the shortest (i.e. most newly divided) cells (**Fig. 2b bottom-left and Extended Data Fig. 2b)**. For further quantification, the fluorescence intensities of the FDAAs were normalized and plotted against their relative positions along the cell length for a subset of cells, from roughly the middle of their cell cycles. As in the demograph, the red signal appeared on both sides of the green signal, confirming bidirectional midcell elongation in *C. crescentus* (**Fig. 2b bottom-right)**.

Contrastingly, in *A. excentricus*, the first, red FDAA signal appeared only on one side of the midcell region, whereas the second, green signal appeared at the midcell region, demonstrating unidirectional PG synthesis (**Fig. 2c and Extended Data Fig. 2b**). To determine whether the unidirectional midcell elongation observed in *A. excentricus* consistently proceeds towards the new pole, we conducted dual short-pulse FDAA labeling experiments in *A. excentricus* cells in which the old poles were marked. For this, we utilized the dimorphic cell cycle of this species, which features regulated changes in morphology and surface adhesion within the context of the cell cycle[31,32]. Specifically, cells produce a holdfast polysaccharide adhesin at the old pole during cell cycle progression, which can be used as an old-pole marker through labeling with fluorescent

wheat germ agglutinin (WGA) lectin. Dual short-pulse FDAA labeling in *A. excentricus* cells with WGA-labeled holdfasts showed that the first FDAA signal was always on the new-pole side of the second FDAA signal (**Fig. 2d**). These results demonstrate that *C. crescentus* has a bidirectional midcell elongation mode while *A. excentricus* has a unidirectional midcell elongation mode in which PG synthesis proceeds towards the new pole (**Fig. 2e**).

The *A. excentricus* class B PG synthase PBP2 localizes to sites of new PG synthesis

To understand the evolutionary origins of unidirectional midcell elongation in *A. excentricus*, we investigated the potential molecular determinants driving this novel elongation mode. Bioinformatic analysis using *C. crescentus* PBP2 and PBP1a as queries revealed a limited repertoire of PG synthases in *A. excentricus*: three class A PBPs, including two homologues of PBP1a (Astex_2378 and Astex_2994) and one homologue of PBP1c (Astex_0196); and two monofunctional class B PBPs – PBP2 and PBP3 (FtsI) (**Extended Data Fig. 3a**). This limited repertoire of PBPs in *A. excentricus,* and the conserved neighborhood architecture of the cell elongation loci in *C. crescentus* and *A. excentricus* (**Extended Data Fig. 3b**) suggested that the same canonical elongasome proteins may have evolved to generate different modes of elongation in the two species. Therefore, we hypothesized that localization of PBP2, an essential component of the elongasome, may play a role in the evolution of these different elongation modes.

To investigate the role of PBP2 in midcell elongation, we utilized fluorescent protein fusions to track its subcellular localization. We fused PBP2 to mCherry at its native locus in *A. excentricus* and performed fluorescence microscopy (See Extended Text for validation of the mCherry-PBP2 fusion). Across the population, PBP2 exhibited a patchy localization with enrichment near the midcell (**Fig. 3a**). Quantifying its localization in a large number of cells in a

demograph, or using a population-wide heatmap of subcellular PBP2 localization using the holdfast as a polar marker **(Fig. 3a)**, we found that PBP2 accumulates close to the midcell offset towards the new pole, which is similar to the location of new PG synthesis. To further analyze whether PG synthesis at the midcell coincides with PBP2 localization, we labeled *A. excentricus* cells expressing mCherry-PBP2 with a short pulse of FDAA. Fluorescence microscopy and quantification using a population-wide heatmap and density map of the maximal fluorescence intensities of the mCherry-PBP2 and FDAA signals showed that the FDAA signal overlapped with the mCherry-PBP2 signal (**Fig. 3b and Extended Data Fig. 4a-b**). Together, these data indicate that PBP2 localization correlates with sites of PG synthesis during unidirectional midcell elongation in *A. excentricus*.

To further probe the link of PBP2's distinct localization in *A. excentricus* to its novel mode of cell elongation, we investigated PBP2 localization in *C. crescentus*, which exhibits bidirectional elongation from the midcell[23]. Using a GFP fusion to PBP2 at its native locus in *C. crescentus*, we observed that GFP-PBP2 displayed a dispersed distribution throughout the cell cycle in *C. crescentus*, consistent with previous studies[33], and distinct from PBP2 localization in *A. excentricus* (**Fig. 3c and Extended Data Fig. 4c-d**). To determine whether PBP2 colocalizes with sites of PG synthesis in *C. crescentus*, we performed short-pulse FDAA labeling in cells expressing GFP-PBP2. Fluorescence microscopy and population-level quantification of cells in a demograph revealed that, unlike in *A. excentricus*, *C. crescentus* PBP2 did not show significant enrichment at the midcell, and the FDAA labeling did not overlap with the GFP-PBP2 signal (**Fig. 3c**). This difference in the localization patterns of PBP2 in *C. crescentus* and *A. excentricus* suggests that the relocalization of PBP2 may be a critical evolutionary step in the divergence of the elongation modes between these two species.

208

209 **PBP2 activity is required for unidirectional elongation at the midcell in *A. excentricus***

210 To understand the functional role of the essential protein PBP2 in the unidirectional midcell
211 elongation of *A. excentricus*, we utilized the β-lactam antibiotic mecillinam, a specific inhibitor of
212 PBP2 transpeptidase activity in *E. coli*[34]. In *C. crescentus,* mecillinam causes cell bulging[35,36],
213 likely through its inhibition of PBP2 activity (**Extended Data Fig. 5a**). To determine the target of
214 mecillinam in *A. excentricus*, we conducted competition assays with the β-lactam Bocillin FL, a
215 fluorescent penicillin that covalently binds all PBPs. Using Bocillin gel analysis, we found that
216 mecillinam predominantly inhibited binding of Bocillin to PBP2, even at high concentrations (100
217 $\mu g\,ml^{-1}$), while other PBPs in *A. excentricus* were only partially affected (**Extended Data Fig. 5b**).
218 These results indicate that mecillinam is a suitable tool to investigate the role of PBP2 in cell
219 elongation in *A. excentricus*.

220 To analyze the effect of PBP2 inhibition on cell elongation, we conducted a FDAA pulse-
221 chase experiment in *A. excentricus* cells expressing ZapA-sfGFP, with or without mecillinam. We
222 labeled whole-cell PG with FDAA over two generations without mecillinam, followed by a wash
223 to remove excess FDAA, and a chase period with or without mecillinam for 120 min. In untreated
224 cells, we found robust FDAA signal loss on the new pole side of the ZapA-sfGFP signal, consistent
225 with unidirectional elongation at the midcell (**Fig. 4a, left**). In contrast, FDAA signal loss in
226 mecillinam-treated cells was observed in bulges on the new pole side of the cell (**Fig. 4a, right**).
227 To quantify the FDAA signal loss and cell bulging upon mecillinam treatment, we measured the
228 subcellular localization of these bulges in relation to the fluorescence signals of ZapA and FDAA
229 in a population-wide analysis. We plotted these features relative to the cell center, generating
230 ShapePlots[37] for the whole population (**Fig. 4b, right panels**), as well as for four categories binned

by cell length. Bulging was detected consistently on the new pole side of the midcell across all four categories, with its position shifting closer to midcell as cells progressed through the cell cycle and approached division **(Fig. 4b, left panels**). These analyses confirmed that bulging occurred primarily on the new pole side of the midcell in *A. excentricus*, i.e. at the site of midcell elongation (**Fig. 4b, top panels**). Furthermore, loss of FDAA signal peaked at this site, suggesting that the bulging may be a result of abnormal PG synthesis at the midcell when PBP2 is inhibited (**Fig. 4b, bottom panels**). Together, these results suggest that PBP2 activity is required for the regulation of elongasome activity at the midcell – both to promote unidirectional PG synthesis towards the new pole, and to prevent bulging.

To further analyze PBP2's role in the directionality of midcell elongation in *A. excentricus*, we conducted dual short-pulse experiments using two differently colored FDAAs in the presence or absence of mecillinam (**Fig. 4c**). In untreated cells, sequential FDAA labeling showed the first, red signal on only one side of the second, green signal, consistent with midcell elongation towards the new pole (**Fig. 4c, left panels**). However, in mecillinam-treated cells, both FDAA signals were distributed diffusely at the site of bulging, confirming the loss of directionality in PG synthesis upon PBP2 inhibition (**Fig. 4c, right panels).** Quantification of mean fluorescence intensities showed reduced FDAA incorporation in cells treated with mecillinam (**Fig. 4d**), consistent with the main transpeptidase of the cell being inhibited. Overall, these observations demonstrate that the inhibition of PBP2 activity severely disrupts the coordination of PG synthesis, leading to bulging at the site of the elongasome, and loss of the novel unidirectional midcell elongation mode of *A. excentricus*. These findings confirm our hypothesis that PBP2's localization and activity evolved together with the evolution of unidirectional midcell elongation in *A. excentricus,* with the enzyme serving as a key organizer of the directionality of elongasome activity in this species.

Diverse modes of midcell elongation within and beyond the *Caulobacteraceae* family

To determine the elongation modes in other *Caulobacteraceae*, we analyzed other species in the genera *Asticcacaulis*, *Phenylobacterium*, *Brevundimonas,* and *Caulobacter* using pulse-chase experiments with FDAA (**Fig. 5a**). To analyze the patterns of FDAA labeling loss across populations of pulse-chased cells, we generated demographs for each species (**Fig. 5b**). Smaller cells of all six species showed a loss of signal at one of their poles, which likely corresponds to a recent division (**Fig. 5b, white stars**). In longer cells, the loss of FDAA labeling during the chase period was located near the midcell, corresponding to midcell elongation at the future site of cell division, or indeed to cell division itself (**Fig. 5b**). In *C. crescentus*, *C. henricii,* and *B. diminuta* the loss of FDAA labeling was located near the midcell, progressing symmetrically towards both cell poles. This observation is consistent with PG synthesis in *C. crescentus* occurring bidirectionally from the midcell region in stalked cells[23] (**Fig. 1b-d, Fig. 2, and Fig. 5c-d**). In contrast, the loss of FDAA labeling during the chase period in *A. excentricus*, *A. biprosthecum* and *P. conjunctum*, started in the midcell region but trended towards the left of the demograph (**Fig. 5b, red arrows)**.

The loss of FDAA predominantly towards one pole in *A. biprosthecum* and *P. conjunctum* suggests a unidirectional elongation mode in these species, similar to *A. excentricus*. To further investigate this, we performed pulse-chase FDAA labeling and time-lapse microscopy in *A. biprosthecum* (**Fig. 6a**). Interestingly, kymograph analysis in this species revealed not only unicellular midcell elongation towards the new pole, as in *A. excentricus,* but also an additional site of elongation at the new pole itself (**Fig. 6b and Extended Data Fig. 6**). This observation suggests that *A. biprosthecum* elongates through yet another novel mode – a combination of polar

277 elongation and unidirectional midcell elongation. To further analyze this mode of cell elongation,
278 we sequentially added differently colored FDAAs during short pulses (5% of a generation time,
279 **Fig. 6c**). Demograph and fluorescence profile analyses revealed that the second, green FDAA
280 signal was present at both the pole and the midcell, while the first, red signal was located mainly
281 at the pole. At the pole, the second, green signal appeared at the tip, while the red signal was
282 positioned just adjacent away from the tip, indicating apical elongation (**Fig. 6d-e and Extended**
283 **Data Fig. 6**). Interestingly, the population-level demographs showed that the FDAA signals at the
284 pole were present throughout the cell cycle, whereas signals at the midcell appeared only in longer
285 cells. This pattern indicates a sequence of polar cell elongation early in the cell cycle followed by
286 unidirectional midcell elongation closer to the time of division. The observation of both polar and
287 unidirectional midcell elongation modes in *A. biprosthecum* underscores the diverse range of cell
288 elongation mechanisms within the *Caulobacteraceae* family.

289 Given the diversity of elongation modes observed even within closely related species (**Fig.**
290 **5b-d**), we questioned whether unidirectional midcell elongation was a rare occurrence limited to
291 the *Caulobacteraceae* family or if it could be observed in other species as well. We therefore
292 extended our investigation to the more distantly related *R. capsulatus*, a member of the
293 alphaproteobacterial order *Rhodobacterales*. We performed pulse-chase FDAA labeling and time-
294 lapse microscopy as before (**Fig. 6a and 6f and Extended Data Fig. 7**). Kymograph analysis
295 showed that the loss of FDAA labeling in *R. capsulatus* originated from the division plane and
296 predominantly moved unidirectionally towards one of the cell poles, suggesting unidirectional
297 midcell elongation. To further investigate the *R. capsulatus* cell elongation mode, we performed a
298 dual short-pulse experiment and with two differently colored FDAAs (**Fig. 6c**). Demograph and
299 fluorescence profile analyses revealed that the first FDAA signal in *R. capsulatus* was only on one

side of the second FDAA signal, towards one of the cell poles (**Fig. 6g-h**). These results show that *R. capsulatus* also exhibits unidirectional elongation from the midcell, similar to the pattern observed in *A. excentricus*. This finding indicates that unidirectional midcell elongation is not restricted to the *Caulobacteraceae* family and suggests that this growth mode may be more widespread within the Alphaproteobacteria.

Overall, the diversity of cell elongation modes identified in this study suggests that there may be more novel modes to discover among bacteria. Our findings also emphasize the need for further exploration of the evolutionary transitions, such as PBP2 relocalization, that may underlie these differences.

DISCUSSION

The existence of different elongation modes in bacteria has been known for decades[38], but the mechanisms behind their evolution have remained unknown, largely due to research bias towards a few, distantly related model organisms. In parallel, there has been an assumption that closely related species share similar elongation mechanisms, hampering the study of divergence at shorter evolutionary scales. In this study, we challenge this assumption by revealing significant differences in the elongation strategies of closely related species within the *Caulobacteraceae* family. Our findings indicate that evolutionary changes in cell elongation can occur more frequently and at shorter evolutionary timescales than previously thought, opening new avenues for research into the evolution of bacterial growth and morphogenesis.

Among the *Caulobacteraceae*, the diversity and novelty of elongation modes we observe - ranging from bidirectional midcell elongation in *C. crescentus, C. henricii and B. diminuta*, to the newly described unidirectional midcell elongation in *A. excentricus* and *P. conjunctum* as well as

the combination of polar and unidirectional midcell elongation in *A. biprosthecum* (**Fig. 1b, Fig. 5 and Fig. 6**), indicate remarkable evolutionary flexibility. They suggest a capacity for closely related species to adapt their elongation mechanisms, possibly in response to evolutionary pressures such as nutrient availability, morphological constraints, competition, predation, etc. It is already known that bacteria can regulate their elongation patterns in response to environmental changes. For instance, *Streptomyces* cells can shift their elongation mechanisms in response to metabolic cues, allowing exploratory growth[39,40]. Meanwhile, *Salmonella typhimurium* encodes two differentially regulated elongasomes, one of which is specialized for pathogenesis, functioning under acidic, intracellular conditions, with slower PG synthesis that may help coordinate cell elongation with host metabolism (although the spatial pattern of elongation remains the same)[41]. Many other bacterial species suppress the highly conserved divisome, using only elongation to produce a filamentous morphology to overcome a range of environmental constraints[42-44]. Finally, within the *Caulobacteraceae*, stalk elongation is a well-known response to nutrient limitation, although this specialized mode of PG synthesis at the stalk site is independent of the core elongasome that drives vegetative growth in the cell[31,45,46]. It would be intriguing to explore whether *A. excentricus* and related species similarly adjust their core elongation modes in response to environmental conditions. Future studies on this topic may shed light on the selective pressures that have led to the divergent elongation modes among the *Caulobacteraceae*.

The plasticity of cell elongation strategies is evident not only under different environmental conditions, but even within a single cell under different regulatory states. For instance, among the *Caulobacteraceae*, the transition from dispersed elongation in the swarmer cell to localized cell elongation at the midcell (**Fig. 1**) demonstrates how elongasome components may be modulated by the cell cycle. Even in *E. coli,* which predominantly grows through dispersed elongation along

its lateral walls, the elongasome-specific PG synthase PBP2 shows a cell-cycle dependent enrichment at the midcell prior to division, coinciding with a burst of midcell elongation[47]. Gram-positive coccoid bacteria such as *S. aureus* offer yet another example of the flexibility of the PG synthesis machinery, which functions both peripherally and for septal sidewall synthesis in these bacteria[48]. These observations underscore that elongation modes are not static in cells, but rather dynamically adaptable through regulatory networks controlling cell growth. Evolutionary forces may drive changes in bacterial elongation by modulating existing molecular mechanisms rather than by introducing new ones.

In this study, we provide evidence of novel cell elongation modes beyond the *Caulobacteraceae* (**Fig. 5c**). Indeed, we discovered that *R. capsulatus* demonstrates unidirectional midcell elongation similar to *A. excentricus* (**Fig. 6f-h**). To understand the evolutionary context of this surprising discovery, we searched the literature for previous reports of elongation modes among the *Rhodobacterales* and found that *Rhodobacter sphaeroides* demonstrates bidirectional midcell elongation[49]. Meanwhile, in another branch of the Alphaproteobacteria, the loss of the key elongation proteins MreB and PBP2 among members of the *Rhizobiales* has coincided with the evolution of polar elongation (**Fig. 5c**), further emphasizing the evolutionary plasticity of bacterial elongation systems[9]. Nonetheless, the conservation of elongasome clusters such as *pbp2/rodA* across species with different elongation modes such as *E. coli, C. crescentus,* and *A. excentricus* (**Extended Data Fig. 3**), suggests that evolutionary changes in elongation modes stem not only from changes in gene content, but also from differences in the regulation, localization or activity of these conserved proteins.

Here, in characterizing the molecular determinants of unidirectional midcell elongation in *A. excentricus*, we discovered that the PG synthase PBP2 is central to the regulation of this

369 elongation strategy. In contrast to its dispersed localization in *C. crescentus*, PBP2 in *A.*
370 *excentricus* concentrates at the midcell, and is required for unidirectional PG synthesis. Upon
371 inhibition of PBP2, cells exhibit abnormal PG synthesis leading to bulging at the midcell
372 elongation site. These results suggest that changes in the specific localization of key enzymes such
373 as PBP2 may be associated with the evolution of distinct cell elongation strategies, enabling
374 bacteria to respond to broader pressures acting on morphology and growth. Notably, in *C.*
375 *crescentus*, PBP2 shifts to the midcell under osmotic stress, illustrating that its localization is
376 subject to regulation both by environmental cues and evolutionary processes[33].

377 Beyond PBP2, other proteins like FtsZ play versatile roles in regulating localized PG
378 synthesis across bacteria[50]. In *C. crescentus*, FtsZ depletion results in dispersed cell elongation[23],
379 while in *Bacillus subtilis*, FtsZ can position itself at the midcell during vegetative growth or closer
380 to the poles for sporulation[51], highlighting its flexibility in regulating PG synthesis for different
381 growth modes. Another interesting example is the conserved outer membrane lipoprotein PapS,
382 which in *Rhodospirillum rubrum* forms molecular cages that confine elongasomes to induce
383 asymmetric cell elongation[52]. The diversity of mechanisms by which bacteria spatially regulate
384 growth using conserved proteins supports the idea that evolution likely acts by altering the function
385 of existing proteins rather than by introducing new genes. In the future, it will be of interest to
386 determine what scaffolding mechanisms are at play in *A. excentricus* and *A. biprosthecum*, driving
387 the unique localization and directionality of PBP2 in their elongasomes.

388 The observation of diverse elongation mechanisms among bacteria raises the fundamental
389 question of the function of such diversity. Why do some species like *A. excentricus* evolve
390 unidirectional elongation, while others maintain dispersed, bidirectional or polar growth
391 mechanisms? What evolutionary factors drive these changes? It is clear that midcell and polar

392 elongation are widely distributed in the Alphaproteobacteria (**Fig. 5c**), suggesting that localized
393 modes of elongation may be ancestral within this class. However, the distribution of elongation
394 modes in our phylogenetic analysis of the *Caulobacteraceae* (**Fig. 5c-d**) suggests that their
395 evolution is likely shaped by multiple, independent events, implying a high degree of phenotypic
396 plasticity in the regulation of localized elongation modes. In particular, the midcell, directional
397 elongation identified in the current study is observed in *Asticcacaulis* and *Phenylobacterium*, but
398 absent in members of *Caulobacter* and *Brevundimonas*, indicating that this growth mode has been
399 gained and/or lost at least twice among the *Caulobacteraceae* (**Fig. 5d**). In light of this observed
400 phenotypic diversity, it is intriguing to consider whether localized elongation itself may be a
401 broadly adaptive strategy that bacteria have evolved, allowing greater plasticity under changing
402 evolutionary pressures than dispersed elongation (although these co-exist in many species). Deeper
403 understanding of the diversity of elongation modes among other branches of bacteria should
404 provide further insights into the prevalence and ancestry of localized, dispersed, and septal modes
405 of elongation, helping to identify selective pressures that shape the evolution of growth mode
406 strategies.

407 Additionally, the evolution of distinct elongation modes has implications for the evolution
408 of bacterial morphology. *C. crescentus*, *A. excentricus*, and *A. biprosthecum* display striking
409 morphological differences, especially in the positioning of their stalks[32]. This raises the possibility
410 that their distinct elongation modes and stalk positioning mechanisms may have co-evolved. In all
411 three species, the site of stalk synthesis corresponds to the region of the oldest PG in the swarmer
412 cell, as it differentiates into a stalked cell. Could the elongation mechanisms of these species thus
413 be driving the placement of their cellular structures? If future studies find this to be true, it would

suggest that elongation modes and cellular morphologies are intricately linked, with changes and selective pressures on one likely to influence the other over evolutionary time.

In summary, the fundamental finding of this study is that bacterial elongation modes are more diverse than previously thought, even at relatively short evolutionary scales. This challenges the assumption that closely related species share similar elongation modes – an assumption that has prevailed largely because we have not had the right tools to explore the diversity of bacterial elongation modes, even at close evolutionary distances from well-studied model organisms. Combining spatiotemporal analyses of PG synthesis using FDAAs alongside genetic and evolutionary approaches now allows a reexamination of previous assumptions about cell elongation modes across bacterial clades. Consequently, we expect these results to be at the forefront of a paradigm shift in our understanding of the diversity of bacterial cell elongation, its regulation and evolution.

Methods

Bacterial strains and growth conditions

All bacterial strains used in this study are listed in **Table S1**. *C. crescentus, B. diminuta,* and *C. henricii were grown at* 30°C in Peptone Yeast Extract (PYE) medium[53]. *A. excentricus*, *A. biprosthecum* and *P. conjunctum* were grown at 26°C in PYE. *R. capsulatus* SB1003 cells were grown at 30°C in PYS (3 g l^{-1} peptone, 3 g l^{-1}yeast extract, 2 mM $MgSO_4$, 2 mM $CaCl_2$) medium[54]. The culture medium was supplemented with antibiotics as necessary at the following concentrations (µg ml^{-1}; liquid/solid medium): spectinomycin (50/100), kanamycin (5/20), gentamicin (0.5/5), and with sucrose at 3% (w/v) for cloning procedures. For microscopy analysis, cells were grown either from a single colony or from frozen stock. Serial dilutions (1:10, 1:50, 1:100, and 1:1000) were made, and cultures were grown overnight at 26°C or 30°C with shaking at 220 rpm before being imaged in mid-exponential phase. *E. coli* strains used in this study were grown in liquid lysogeny broth (LB) medium at 37°C supplemented with antibiotics or supplements as necessary (diaminopimelic acid (DAP) 300 µg ml^{-1}, kanamycin 50 µg ml^{-1}, spectinomycin 100 µg ml^{-1}, gentamicin 15 µg ml^{-1} and streptomycin 30 µg ml^{-1}). Strains were maintained on LB plates at 37°C supplemented with antibiotics as necessary (kanamycin 50 µg ml^{-1}, spectinomycin 100 µg ml^{-1} and streptomycin 30 µg ml^{-1}).

Plasmid constructions and cloning procedures

All plasmids used in this study were cloned using standard molecular biology techniques and are listed in **Table S2**. PCRs were performed using *A. excentricus* CB48 WT or mutant genomic DNA as template. Gibson assemblies were performed using the Gibson Assembly® Master Mix from NEB[55]. Sequences of the primers used are available upon request.

452 In-frame deletions and fluorescent fusions in *A. excentricus* were obtained by double
453 homologous recombination and sucrose counterselection, as previously described[56]. For deletions,
454 700-bp fragments from the upstream and downstream regions of the gene to be deleted were
455 amplified by PCR. For the N-terminal mCherry fusion to PBP2, 500-bp of the upstream and N-
456 terminus regions of the *pbp2* gene were amplified by PCR, along with the *mCherry* gene. PCR
457 fragments were gel-purified and cloned using Gibson assembly into the suicide vector pNPTS139
458 that had been digested by *EcoRI* and *HindIII*. The pNPTS139-based constructs were transformed
459 into *E. coli* DH5α cells, verified by PCR sequencing, and then introduced into *A. excentricus* via
460 biparental mating using the dap$^-$ *E. coli* strain WM3064 (YB7351)[57]. The pGFPC-5 plasmid with
461 *egfp* replaced by *sfgfp* was used for generating the C-terminal sfGFP fusion to ZapA in *A.*
462 *excentricus*. Proper chromosomal integration or gene replacement was verified by colony PCR and
463 Sanger sequencing.

464

465 **Fluorescent D-amino acids (FDAAs)**

466 In this study, three different FDAAs were used: HADA (7-hydroxycoumarin-3-carboxylic
467 acid-D-alanine; emission peak ~407nm), BADA (BODIPY FL-D-alanine; emission peak
468 ~515nm), and TADA (TAMRA-D-alanine; emission peak ~578nm). FDAA stock solutions were
469 prepared in anhydrous DMSO at a concentration of 100 mM. In fluorescent images and
470 demographs, the FDAAs are false colored in green or red depending on the experiment, as detailed
471 in the figure legends.

472

473 **FDAA pulse-chase experiments**

To label whole cells, 250 μM TADA or BADA was added to early exponential phase cells (OD600 ~0.1). The cells were allowed to grow for two generations, after which they were washed three times with appropriate medium to remove excess FDAA from the medium. Subsequently, growth was monitored following the wash using time-lapse microscopy, or cells were allowed to grow for half their generation times and imaged using phase and fluorescence microscopy to generate demographs (see "Image analysis" below).

For the FDAA pulse-chase experiments with mecillinam treatment, bacterial cells (OD600 ~0.1) were incubated with 250 μM TADA over two generations. Excess FDAA was removed by centrifugation at 6,000g for 3 min, and the cells were washed three times with PYE. Cell pellets were then resuspended in PYE with or without 50 μg ml^{-1} mecillinam, grown for one additional doubling time, and imaged using phase and fluorescence microscopy.

Dual short-pulse labeling with FDAAs

For dual short-pulse FDAA labeling in *C. crescentus*, HADA was added to early exponential phase cells (OD600 ~0.25) to a final concentration of 1 mM. The cells were grown in PYE at 30°C for 5% of their doubling time (5 minutes). Then, the excess dye was removed by centrifugation at 6,000g for 3 min, and cells were washed 3 times with PYE. The cell pellets were resuspended in PYE, and the cells were allowed to grow for an additional 15% of their generation time (15 minutes) in fresh PYE. BADA was then added to the culture medium to a final concentration of 1 mM. The cells were grown for an additional 5% of their doubling time for sequential labeling. Excess BADA was then removed by centrifugation at 6,000g for 3 min, and cells were washed 3 times with PYE. The labeled cells were resuspended in PYE and imaged with phase and fluorescence microscopy.

For dual short-pulse FDAA labeling in *A. excentricus*, TADA was added to early exponential phase cells (OD600 ~0.25) to a final concentration of 500 µM. The cells were grown in PYE at 26°C for 5% of their doubling time (6 minutes). Then, excess TADA was removed by centrifugation at 6,000g for 3 min, and cells were washed 3 times with PYE. The cell pellets were resuspended in PYE, and the cells were allowed to grow for an additional 15% of their generation time (18 minutes) in fresh PYE at 26°C. BADA was then added to the culture medium to a final concentration of 500 µM. The cells were then grown for an additional 5% of their doubling time for sequential labeling. Excess BADA was removed by centrifugation at 6,000g for 3 min, and cells were fixed in ethanol 70% for 1 hour. The fixed cells were washed with PYE twice and imaged with phase and fluorescence microscopy.

For dual short-pulse FDAA labeling in *A. biprosthecum*, TADA was added to early exponential phase cells (OD600 ~0.25) to a final concentration of 250 µM. The cells were grown in PYE at 26°C for 5% of their doubling time (7 min). Then, excess TADA was removed by centrifugation at 6,000g for 3 min, and cells were washed 3 times with PYE. The cell pellets were resuspended in PYE, and the cells were allowed to grow for an additional 15% of their generation time (21 minutes) in fresh PYE at 26°C. BADA was then added to the culture medium to a final concentration of 250 µM. The cells were then grown for an additional 5% of their doubling time for sequential labeling. Excess BADA was removed by centrifugation at 6,000g for 3 min, and cells were fixed in ethanol 70% for 1 hour. The fixed cells were washed with PYE twice and imaged with phase and fluorescence microscopy.

For dual short-pulse FDAA labeling in *R. capsulatus*, TADA was added to early exponential phase cells (OD600 ~0.25) to a final concentration of 250 µM. The cells were grown in PYS at 30°C for 5% of their doubling time (6 min). Then, excess TADA was removed by

centrifugation at 6,000g for 3 min, and cells were washed 3 times with PYS. The cell pellets were resuspended in PYS, and the cells were allowed to grow for an additional 15% of their generation time (18 minutes) in fresh PYS at 26°C. BADA was then added to the culture medium to a final concentration of 250 µM. The cells were then grown for an additional 5% of their doubling time for dual sequential labeling. Excess BADA was removed by centrifugation at 6,000g for 3 min, and cells were fixed in ethanol 70% for 1 hour. The fixed cells were washed with PYS twice and imaged with phase and fluorescence microscopy

To orientate *A. excentricus* and *A. biprosthecum* cells using the old pole, holdfasts were detected with CF®405S conjugated wheat germ agglutinin (CF®405S WGA, 0.5 µg ml^{-1} final concentration) since WGA binds specifically to the acetylglucosamine residues present in their holdfasts[58].

For FDAA dual short-pulse labeling in the presence of mecillinam, *A. excentricus* cells (OD_{600} ~0.25) were treated with mecillinam (50 µg ml^{-1}) for 120 min. The treated cells were labeled with FDAAs as described above, but in presence of 50 µg ml^{-1} mecillinam for two sequential pulses of 5 min.

Single short-pulse labeling with FDAA in *A. excentricus* and *C. crescentus* PBP2 fluorescent fusion cells

BADA and TADA were added to early exponential phase (OD600 ~0.25) *C. crescentus gfp-pbp2* and *A. excentricus mCherry-pbp2* cells, to a final concentration of 250 µM. The *C. crescentus* and *A. excentricus* cells were grown in PYE at 30°C and at 26°C, respectively, for 5% of their doubling time. Excess FDAA was removed by centrifugation at 6,000g for 3 min and cells

were fixed with 70% ethanol for 1 hour. Cells were washed 2 times with PYE, and labeled cells were then resuspended in PYE and imaged with phase and fluorescence microscopy.

Microscopy

For light microscopy analysis, 24 mm × 50 mm coverslips (#1.5) were used as imaging supports for an inverted microscopy system. An agarose pad was made of 1% SeaKem LE Agarose (Lonza, Cat. No. 50000) in dH2O. Cell samples were loaded onto the coverslips. Then, an 8 mm × 8 mm × 2 mm (length, width, thickness) dH2O-agar pad was laid on top of the cells. The coverslip–pad combination was placed onto a customized slide holder on microscopes with the pad facing upwards.

For time-lapse, 1 µl FDAA-labeled cells were spotted onto pads made of 0.7% Gelrite (Research product international, CAS. No. 71010-52-1) in PYE for *C. crescentus*, *A. excentricus* and *A. biprosthecum* cells and topped with a glass coverslip. 1 µl FDAA-labeled *R. capsulatus* cells were spotted onto pads made of 0.7% Gelrite in PYS and topped with a glass coverslip. The coverslip was sealed with VALAP (vaseline, lanolin, and paraffin at a 1:1:1 ratio).

Images were recorded with inverted Nikon Ti-E or Ti2 microscopes using a Plan Apo 60X 1.40 NA oil Ph3 DM objective with DAPI/FITC/Cy3/Cy5 or CFP/YFP/mCherry filter cubes and a Photometrics Prime 95B sCMOS camera. Images were processed with the NIS Elements software (Nikon).

Image analysis

Cell dimensions were obtained using FIJI[59] and the plugin MicrobeJ[37]. To quantitatively analyze the pattern of FDAA loss in pulse-chase experiments, or of FDAA incorporation during

dual short-pulse experiments, we generated kymographs and/or demographs using the MicrobeJ results interface. In these demographs, each cell is oriented such that the pole with the maximum mean fluorescence is set to the left and cells are aligned at the midcell. Alternatively, where holdfast staining was used, the holdfast signal (old pole) was set to the right. All cells were aligned at the midcell. Using the MicrobeJ demograph tool, 50% of the maximum intensity of each pulse was displayed in the main figures, while the total fluorescence signals are presented in the extended data. Demographs of the pulse-chase experiments of the different *Caulobacteraceae* species show 80% of the maximum fluorescence intensity.

Subcellular localization heatmaps and density maps for mCherry-PBP2 and FDAA foci were generated using MicrobeJ using the "Maxima" detection option. Density map merges were produced by importing each density map into Adobe Illustrator CC 2023 (Adobe Inc.) and manually merging the plots.

To quantitatively analyze the patterns of FDAA loss and cell bulging during pulse-chase experiments with mecillinam treatment, we quantified the subcellular localization of bulges along with the fluorescence intensities of ZapA and TADA. Localization of the bulge was determined using the "feature" option of MicrobeJ. Instead of looking for constriction, we looked for bulging, using the option "inverted" in the feature parameters interface. Using the subcellular localization charts function of the MicrobeJ results interface, we plotted bulge distribution relative to the cell center and generated a ShapePlot based on cell length to localize ZapA fluorescence intensity and FDAA signal loss as a readout for PG synthesis. GraphPad Prism (v. 10.3.0) was used to generate histograms and fluorescence intensity profiles and to perform statistical analysis.

In vitro **mecillinam titration against PBPs**

In vitro mecillinam titration against PBPs was performed with modifications to a previous protocol for PBP detection in *E.* coli[60]. Specifically, *A. excentricus* cells in exponential phase (OD_{600} ~0.5) were harvested by centrifugation at 10,000*g* for 4 min at room temperature. The cell pellets were washed twice with 1 ml PBS (pH 7.4). Cells were then resuspended in 50 µl PBS containing 1, 10, or 100 µg ml^{-1} of the antibiotic, while a reference sample was resuspended in 50 µl PBS without antibiotics. After 4 h of incubation at room temperature, cells were pelleted, washed with PBS, and resuspended in 50 µl PBS containing 5 µg ml^{-1} Boc-FL. Following a 30-min incubation at room temperature, cells were pelleted, washed with 1 ml PBS, and then resuspended in 100 µl PBS. The cells were sonicated on ice using a Branson Sonifier 250 instrument (power setting 60 A, 30 s cycle for three 10 s intervals with 10 s of cooling time between rounds) to isolate the membrane proteome. The membrane pellet was then resuspended in 100 µl PBS and homogenized by sonication (power setting 20 A for 1 s). The protein concentration was measured using a NanoDrop 1000 Spectrophotometer and adjusted to 2.5 mg ml^{-1} using PBS. Proteome samples (20 µl) were dispensed into clean 1.5 ml microcentrifuge tubes, and 10 µl of 2× SDS-PAGE loading buffer was added to each sample. The samples were heated for 5 min at 90 °C to denature the proteins, cooled to room temperature, and then 25 µl of each sample was loaded onto a 4–15% SDS-PAGE precast gel. The gel was rinsed with distilled water three times and scanned using a Gel Doc XR system (Bio-Rad Laboratories, Inc) with a 526 nm short-pass filter.

Phylogenetic analysis of selected Alphaproteobacteria

Whole-genome data were obtained from the genome database maintained by the National Center for Biotechnology Information[61]. From each genome, a set of 37 conserved genes was identified and the translated amino acid sequences aligned and concatenated using Phylosift[62].

Phylogenetic reconstruction with MrBayes[63] used a mixed amino acid model including a four-category approximation of gamma-distributed rate variation and an invariant site category. Two simultaneous Markov chain runs were performed for 3,000,000 generations, discarding the initial 25% for burn-in. The tree was visualized and formatted using iTOL[64].

Bioinformatic analyses and the phylogeny of PBPs

Identification of putative PBPs in *A. excentricus* was performed by BLAST analysis using *C. crescentus* PBP2 and PBP1a as queries. Amino acid sequences of homologues (including from other model organisms) were collected from UniProt (https://www.uniprot.org): PBP5 (BSU00100) in *B. subtilis*, DacD (JW5329), PBP1a (JW3359), PBP1b (JW0145), PBP1c (JW2503), PBP2 (JW0630), PBP3 (JW0082) and MTG (JW3175) in *E. coli*, PBP3 (Astex_1844), PBP2 (Astex_1631), PBP1a (Astex_2994), PBP1c (Astex_0196), PBP1b (Astex_2378) and MTG (Astex_0406) in *A. excentricus*, and PBP3 (CCNA_02643), PBP2 (CCNA_01615), PBPz (CCNA_93685), PBPc (CCNA_03386), PBPx (CCNA_01584), PBP1a (CCNA_01584) and MTG (CCNA_00328) in *C. crescentus*. Sequences were then aligned using MUSCLE v.3.8.31 (Fig. S5.1), and PhyML 3.0 was used to reconstruct the maximum likelihood phylogenetic tree, with automatic model selection by Smart Model Selection (SMS)[65] and Akaike information criterion. Phylogenetic reconstruction was performed by RAxML version 8.2.10[66] with 100 rapid bootstraps replicates to assess node support. The tree was visualized and formatted using iTOL[64]. Taxonomic assignments were based on the taxonomy database maintained by NCBI (https://www.ncbi.nlm.nih.gov/Taxonomy/Browser/wwwtax.cgi).

Genomic organization of the *pbp2* and *mreB* genes

The genomic organization of the *pbp2* and *mreB* operons was analyzed using a combination of annotation, sequence search, and synteny visualization tools. Genome assemblies were first annotated with prokka[67]. The annotated files were organized into folders according to their formats (FAA, FNA, GFF, and GBK). For each FAA file, a BLAST protein database was created using the makeblastdb function, and the FNA files were indexed using samtools. GBK files were separated by contig using a Python script with BioPython's SeqIO library[68] to save each contig as an individual GBK file.

When protein files contained multiple sequences, they were split into individual files using SeqKit[69]. Each protein sequence was then identified by performing a BLAST search against the FAA databases. The blast search results were filtered to retain the first hit. Locus tags from the BLAST hits were extracted from the GFF files and converted to BED format. For analyses requiring extended genomic regions, the coordinates were expanded by 5000 bp upstream and downstream using bedtools slop.

To conduct synteny analysis, locus tags from the BED regions were extracted, and the corresponding protein sequences were retrieved from the FAA files using SeqKit[69]. A BLAST database was generated from these sequences, followed by an all-vs-all BLAST search. The matches were clustered based on sequence identity using the MCL algorithm[70], grouping homologous sequences.

Clusters were assigned specific colors, and the GBK files were edited by adding these colors for each corresponding locus tag. Synteny diagrams were created with EasyFig[71], with coding regions represented as arrows and other genomic features (e.g., tRNA and rRNA genes) depicted as rectangles. Multiple synteny figures were arranged in the desired order and merged using Adobe Illustrator CC 2023 (Adobe Inc.).

Illumina sequencing methods

Illumina sequencing was performed by SeqCenter in Pittsburgh, PA.

Sample libraries were prepared using the Illumina DNA Prep kit and IDT 10bp UDI indices, and sequenced on an Illumina NextSeq 2000, producing 2x151bp reads. Demultiplexing, quality control and adapter trimming were performed with bcl-convert (v3.9.30).

Variant Calling Methods

Illumina-generated 2x151bp paired-end read data was used as the input for variant calling against the provided GenBank AC48 reference. Variant calling was carried out using Breseq (v0.37.1) under default settings[72]. Mutations were confirmed by Sanger sequencing.

Data Availability

The data that support the findings of this study are available from the corresponding author on request.

Acknowledgments

The NIH supported this work with grants R35GM122556 to Y.V.B. and R35GM136365 to M.S.V. Y.V.B. is also supported by a Canada 150 Research Chair in Bacterial Cell Biology. M.D. was in part supported by a postdoctoral fellowship from the Swiss National Science Foundation (projet #P2GEP3_191489, and P500PB_206676). F.J.V. received a Junior 1 and Junior 2 research scholar salary award from the Fonds de Recherche du Québec-Santé. Thanks to Yen-pang Hsu for synthesizing the FDAA. We thank Adrien Ducret for help with MicrobeJ. Many thanks to previous and current Brun Lab members for either providing guidance to the project or proofreading the manuscript.

Author Contributions

M.D., L.Y., and Y.V.B. designed the research. M.D. and L.Y. performed all the experiments, except for the whole-genome sequencing of the fluorescent fusion to *pbp2* strain performed by M.J. and whole-genome sequencing and genome assembly of *A. biprosthecum* and *C. conjunctum* performed by F.P. D.T.K. conducted the phylogenetic analysis of Alphaproteobacteria species. M.D., together with K.A.G., carried out the bioinformatic analyses and the phylogeny of PBPs. M.S.V. contributed fluorescent D-amino acids (FDAAs). M.D., L.Y., V. H. and Y.V.B. analyzed the overall data. M.D., L.Y., V.H., and Y.V.B. wrote the manuscript. M.D., F.J.V., and Y.V.B. acquired funding.

Competing interests

The authors declare no competing interests.

697

Reference

1 Curtis, P. D. & Brun, Y. V. Getting in the loop: regulation of development in Caulobacter crescentus. *Microbiol Mol Biol Rev* **74**, 13-41, doi:10.1128/MMBR.00040-09 (2010).

2 Woldemeskel, S. A. & Goley, E. D. Shapeshifting to Survive: Shape Determination and Regulation in Caulobacter crescentus. *Trends Microbiol* **25**, 673-687, doi:10.1016/j.tim.2017.03.006 (2017).

3 Egan, A. J., Errington, J. & Vollmer, W. Regulation of peptidoglycan synthesis and remodelling. *Nature Reviews Microbiology* **18**, 446-460 (2020).

4 Kysela, D. T., Randich, A. M., Caccamo, P. D. & Brun, Y. V. Diversity Takes Shape: Understanding the Mechanistic and Adaptive Basis of Bacterial Morphology. *PLoS Biol* **14**, e1002565, doi:10.1371/journal.pbio.1002565 (2016).

5 Randich, A. M. & Brun, Y. V. Molecular mechanisms for the evolution of bacterial morphologies and growth modes. *Front Microbiol* **6**, 580, doi:10.3389/fmicb.2015.00580 (2015).

6 Garner, E. C. Toward a Mechanistic Understanding of Bacterial Rod Shape Formation and Regulation. *Annual Review of Cell and Developmental Biology* **37**, null, doi:10.1146/annurev-cellbio-010521-010834 (2021).

7 Egan, A. J., Biboy, J., van't Veer, I., Breukink, E. & Vollmer, W. Activities and regulation of peptidoglycan synthases. *Philosophical Transactions of the Royal Society B: Biological Sciences* **370**, 20150031 (2015).

8 Egan, A. J., Cleverley, R. M., Peters, K., Lewis, R. J. & Vollmer, W. Regulation of bacterial cell wall growth. *The FEBS journal* **284**, 851-867 (2017).

9 Brown, P. J., de Pedro, M. A., Kysela, D. T., Van der Henst, C., Kim, J., De Bolle, X., Fuqua, C. & Brun, Y. V. Polar growth in the Alphaproteobacterial order Rhizobiales. *Proc Natl Acad Sci U S A* **109**, 1697-1701, doi:10.1073/pnas.1114476109 (2012).

10 Cameron, T. A., Anderson-Furgeson, J., Zupan, J. R., Zik, J. J. & Zambryski, P. C. Peptidoglycan synthesis machinery in Agrobacterium tumefaciens during unipolar growth and cell division. *mBio* **5**, e01219-01214, doi:10.1128/mBio.01219-14 (2014).

11 Cameron, T. A., Zupan, J. R. & Zambryski, P. C. The essential features and modes of bacterial polar growth. *Trends in Microbiology* **23**, 347-353, doi:https://doi.org/10.1016/j.tim.2015.01.003 (2015).

12 Kieser, K. J. & Rubin, E. J. How sisters grow apart: mycobacterial growth and division. *Nature Reviews Microbiology* **12**, 550-562, doi:10.1038/nrmicro3299 (2014).

13 Sher, J. W., Lim, H. C. & Bernhardt, T. G. Polar Growth in Corynebacterium glutamicum Has a Flexible Cell Wall Synthase Requirement. *mBio* **12**, e0068221, doi:10.1128/mBio.00682-21 (2021).

14 Williams, M. A., Aliashkevich, A., Krol, E., Kuru, E., Bouchier, J. M., Rittichier, J., Brun, Y. V., VanNieuwenhze, M. S., Becker, A., Cava, F. & Brown, P. J. B. Unipolar peptidoglycan synthesis in the Rhizobiales requires an essential class A penicillin-binding protein. *bioRxiv*, 2021.2003.2031.437934, doi:10.1101/2021.03.31.437934 (2021).

15 Hett, E. C. & Rubin, E. J. Bacterial growth and cell division: a mycobacterial perspective. *Microbiol. Mol. Biol. Rev.* **72**, 126-156 (2008).

16 Baranowski, C., Rego, E. H. & Rubin, E. J. The dream of a Mycobacterium. *Gram-Positive Pathogens*, 1096-1106 (2019).

17 Canepari, P., Signoretto, C., Boaretti, M. & Lleò, M. D. M. Cell elongation and septation are two mutually exclusive processes in Escherichia coli. *Archives of microbiology* **168**, 152-159 (1997).

18 Kieser, K. J. & Rubin, E. J. How sisters grow apart: mycobacterial growth and division. *Nature Reviews Microbiology* **12**, 550 (2014).

19 Garner, E. C., Bernard, R., Wang, W., Zhuang, X., Rudner, D. Z. & Mitchison, T. Coupled, circumferential motions of the cell wall synthesis machinery and MreB filaments in B. subtilis. *Science* **333**, 222-225 (2011).

20 Pinho, M. G., Kjos, M. & Veening, J. W. How to get (a)round: mechanisms controlling growth and division of coccoid bacteria. *Nat Rev Microbiol* **11**, 601-614, doi:10.1038/nrmicro3088 (2013).

21 Philippe, J., Vernet, T. & Zapun, A. The elongation of ovococci. *Microb Drug Resist* **20**, 215-221, doi:10.1089/mdr.2014.0032 (2014).

22 Caccamo, P. D. & Brun, Y. V. The Molecular Basis of Noncanonical Bacterial Morphology. *Trends in Microbiology* **26**, 191-208, doi:10.1016/j.tim.2017.09.012 (2018).

23 Aaron, M., Charbon, G., Lam, H., Schwarz, H., Vollmer, W. & Jacobs-Wagner, C. The tubulin homologue FtsZ contributes to cell elongation by guiding cell wall precursor synthesis in Caulobacter crescentus. *Molecular microbiology* **64**, 938 (2007).

24 Leifson, E. HYPHOMICROBIUM NEPTUNIUM SP. N. *Antonie Van Leeuwenhoek* **30**, 249-256, doi:10.1007/bf02046730 (1964).

25 Wali, T. M., Hudson, G. R., Danald, D. A. & Weiner, R. M. Timing of swarmer cell cycle morphogenesis and macromolecular synthesis by Hyphomicrobium neptunium in synchronous culture. *J Bacteriol* **144**, 406-412, doi:10.1128/jb.144.1.406-412.1980 (1980).

26 Badger, J. H., Hoover, T. R., Brun, Y. V., Weiner, R. M., Laub, M. T., Alexandre, G., Mrázek, J., Ren, Q., Paulsen, I. T., Nelson, K. E., Khouri, H. M., Radune, D., Sosa, J., Dodson, R. J., Sullivan, S. A., Rosovitz, M. J., Madupu, R., Brinkac, L. M., Durkin, A. S., Daugherty, S. C., Kothari, S. P., Giglio, M. G., Zhou, L., Haft, D. H., Selengut, J. D., Davidsen, T. M., Yang, Q., Zafar, N. & Ward, N. L. Comparative genomic evidence for a close relationship between the dimorphic prosthecate bacteria Hyphomonas neptunium and Caulobacter crescentus. *J Bacteriol* **188**, 6841-6850, doi:10.1128/jb.00111-06 (2006).

27 Kuru, E., Hughes, H. V., Brown, P. J., Hall, E., Tekkam, S., Cava, F., de Pedro, M. A., Brun, Y. V. & VanNieuwenhze, M. S. In Situ probing of newly synthesized peptidoglycan in live bacteria with fluorescent D-amino acids. *Angew Chem Int Ed Engl* **51**, 12519-12523, doi:10.1002/anie.201206749 (2012).

28 Kuru, E., Radkov, A., Meng, X., Egan, A., Alvarez, L., Dowson, A., Booher, G., Breukink, E., Roper, D. I., Cava, F., Vollmer, W., Brun, Y. & VanNieuwenhze, M. S. Mechanisms of Incorporation for D-Amino Acid Probes That Target Peptidoglycan Biosynthesis. *ACS Chem Biol* **14**, 2745-2756, doi:10.1021/acschembio.9b00664 (2019).

29 Woldemeskel, S. A., McQuillen, R., Hessel, A. M., Xiao, J. & Goley, E. D. A conserved coiled-coil protein pair focuses the cytokinetic Z-ring in Caulobacter crescentus. *Mol Microbiol* **105**, 721-740, doi:10.1111/mmi.13731 (2017).

30 Kuru, E., Tekkam, S., Hall, E., Brun, Y. V. & Van Nieuwenhze, M. S. Synthesis of fluorescent D-amino acids and their use for probing peptidoglycan synthesis and bacterial growth in situ. *Nat Protoc* **10**, 33-52, doi:10.1038/nprot.2014.197 (2015).

31 Wagner, J. K. & Brun, Y. V. Out on a limb: how the Caulobacter stalk can boost the study of bacterial cell shape. *Molecular microbiology* **64**, 28-33 (2007).

32 Jiang, C., Brown, P. J., Ducret, A. & Brun, Y. V. Sequential evolution of bacterial morphology by co-option of a developmental regulator. *Nature* **506**, 489-493 (2014).

33 Hocking, J., Priyadarshini, R., Takacs, C. N., Costa, T., Dye, N. A., Shapiro, L., Vollmer, W. & Jacobs-Wagner, C. Osmolality-dependent relocation of penicillin-binding protein PBP2 to the division site in Caulobacter crescentus. *Journal of bacteriology* **194**, 3116-3127 (2012).

34 Legaree, B. A., Daniels, K., Weadge, J. T., Cockburn, D. & Clarke, A. J. Function of penicillin-binding protein 2 in viability and morphology of Pseudomonas aeruginosa. *Journal of antimicrobial chemotherapy* **59**, 411-424 (2007).

35 Koyasu, S., Fukuda, A., Okada, Y. & Poindexter, J. S. Penicillin-binding Proteins of the Stalk of Caulobacter crescentus. *Microbiology* **129**, 2789-2799, doi:https://doi.org/10.1099/00221287-129-9-2789 (1983).

36 Seitz, L. C. & Brun, Y. V. Genetic analysis of mecillinam-resistant mutants of Caulobacter crescentus deficient in stalk biosynthesis. *Journal of bacteriology* **180**, 5235-5239, doi:10.1128/JB.180.19.5235-5239.1998 (1998).

37 Ducret, A., Quardokus, E. M. & Brun, Y. V. MicrobeJ, a tool for high throughput bacterial cell detection and quantitative analysis. *Nat Microbiol* **1**, 16077, doi:10.1038/nmicrobiol.2016.77 (2016).

38 Brown, P. J., Kysela, D. T. & Brun, Y. V. Polarity and the diversity of growth mechanisms in bacteria. *Semin Cell Dev Biol* **22**, 790-798, doi:10.1016/j.semcdb.2011.06.006 (2011).

39 Zambri, M. P., Baglio, C. R., Irazoki, O., Jones, S. E., Garner, E. C., Cava, F. & Elliot, M. A. Bacteria combine polar- and dispersed-growth to power cell elongation and wall width dynamics. *bioRxiv*, 2024.2007.2030.605496, doi:10.1101/2024.07.30.605496 (2024).

40 Jones, S. E., Ho, L., Rees, C. A., Hill, J. E., Nodwell, J. R. & Elliot, M. A. Streptomyces exploration is triggered by fungal interactions and volatile signals. *Elife* **6**, doi:10.7554/eLife.21738 (2017).

41 Castanheira, S. & García-del Portillo, F. Evidence of two differentially regulated elongasomes in Salmonella. *Communications Biology* **6**, 923, doi:10.1038/s42003-023-05308-w (2023).

42 Karasz, D. C., Weaver, A. I., Buckley, D. H. & Wilhelm, R. C. Conditional filamentation as an adaptive trait of bacteria and its ecological significance in soils. *Environmental Microbiology* **24**, 1-17, doi:https://doi.org/10.1111/1462-2920.15871 (2022).

43 Justice, S. S., Hunstad, D. A., Cegelski, L. & Hultgren, S. J. Morphological plasticity as a bacterial survival strategy. *Nat Rev Microbiol* **6**, 162-168, doi:10.1038/nrmicro1820 (2008).

44 Justice, S. S., Hunstad, D. A., Seed, P. C. & Hultgren, S. J. Filamentation by Escherichia coli subverts innate defenses during urinary tract infection. *Proc Natl Acad Sci U S A* **103**, 19884-19889, doi:10.1073/pnas.0606329104 (2006).

45 Billini, M., Biboy, J., Kühn, J., Vollmer, W. & Thanbichler, M. A specialized MreB-dependent cell wall biosynthetic complex mediates the formation of stalk-specific peptidoglycan in Caulobacter crescentus. *PLOS Genetics* **15**, e1007897, doi:10.1371/journal.pgen.1007897 (2019).

46 Wagner, J. K., Galvani, C. D. & Brun, Y. V. Caulobacter crescentus requires RodA and MreB for stalk synthesis and prevention of ectopic pole formation. *J Bacteriol* **187**, 544-553, doi:10.1128/JB.187.2.544-553.2005 (2005).

47 van der Ploeg, R., Verheul, J., Vischer, N. O. E., Alexeeva, S., Hoogendoorn, E., Postma, M., Banzhaf, M., Vollmer, W. & den Blaauwen, T. Colocalization and interaction between elongasome and divisome during a preparative cell division phase in scherichia coli. *Molecular Microbiology* **87**, 1074-1087, doi:https://doi.org/10.1111/mmi.12150 (2013).

48 Reichmann, N. T., Tavares, A. C., Saraiva, B. M., Jousselin, A., Reed, P., Pereira, A. R., Monteiro, J. M., Sobral, R. G., VanNieuwenhze, M. S., Fernandes, F. & Pinho, M. G. SEDS-bPBP pairs direct lateral and septal peptidoglycan synthesis in Staphylococcus aureus. *Nat Microbiol* **4**, 1368-1377, doi:10.1038/s41564-019-0437-2 (2019).

831 49 Lakey, B. D., Alberge, F., Parrell, D., Wright, E. R., Noguera, D. R. & Donohue, T. J. The role of
832 CenKR in the coordination of Rhodobacter sphaeroides cell elongation and division. *mBio*
833 **14**, e00631-00623, doi:doi:10.1128/mbio.00631-23 (2023).

834 50 Randich, A. M. & Brun, Y. V. Molecular mechanisms for the evolution of bacterial morphologies
835 and growth modes. *Frontiers in Microbiology* **6**, doi:10.3389/fmicb.2015.00580 (2015).

836 51 Khanna, K., Lopez-Garrido, J., Sugie, J., Pogliano, K. & Villa, E. Asymmetric localization of the
837 cell division machinery during Bacillus subtilis sporulation. *eLife* **10**, e62204,
838 doi:10.7554/eLife.62204 (2021).

839 52 Pöhl, S., Giacomelli, G., Meyer, F. M., Kleeberg, V., Cohen, E. J., Biboy, J., Rosum, J., Glatter, T.,
840 Vollmer, W., van Teeseling, M. C. F., Heider, J., Bramkamp, M. & Thanbichler, M. An outer
841 membrane porin-lipoprotein complex modulates elongasome movement to establish cell curvature
842 in Rhodospirillum rubrum. *Nature Communications* **15**, 7616, doi:10.1038/s41467-024-51790-z
843 (2024).

844 53 Poindexter, J. S. Biological properties and classification of the Caulobacter group. *Bacteriological*
845 *reviews* **28**, 231 (1964).

846 54 Zappa, S. & Bauer, C. E. The LysR-type transcription factor HbrL is a global regulator of iron
847 homeostasis and porphyrin synthesis in Rhodobacter capsulatus. *Mol Microbiol* **90**, 1277-1292,
848 doi:10.1111/mmi.12431 (2013).

849 55 Gibson, D. G., Young, L., Chuang, R. Y., Venter, J. C., Hutchison, C. A., 3rd & Smith, H. O.
850 Enzymatic assembly of DNA molecules up to several hundred kilobases. *Nat Methods* **6**, 343-345,
851 doi:10.1038/nmeth.1318 (2009).

852 56 Ried, J. L. & Collmer, A. An nptI-sacB-sacR cartridge for constructing directed, unmarked
853 mutations in gram-negative bacteria by marker exchange-eviction mutagenesis. *Gene* **57**, 239-246,
854 doi:10.1016/0378-1119(87)90127-2 (1987).

855 57 Saltikov, C. W. & Newman, D. K. Genetic identification of a respiratory arsenate reductase. *Proc*
856 *Natl Acad Sci U S A* **100**, 10983-10988, doi:10.1073/pnas.1834303100 (2003).

857 58 Merker, R. I. & Smit, J. Characterization of the adhesive holdfast of marine and freshwater
858 caulobacters. *Applied and environmental microbiology* **54**, 2078-2085,
859 doi:10.1128/aem.54.8.2078-2085.1988 (1988).

860 59 Schindelin, J., Arganda-Carreras, I., Frise, E., Kaynig, V., Longair, M., Pietzsch, T., Preibisch, S.,
861 Rueden, C., Saalfeld, S., Schmid, B., Tinevez, J.-Y., White, D. J., Hartenstein, V., Eliceiri, K.,
862 Tomancak, P. & Cardona, A. Fiji: an open-source platform for biological-image analysis. *Nature*
863 *Methods* **9**, 676-682, doi:10.1038/nmeth.2019 (2012).

864 60 Kocaoglu, O. & Carlson, E. E. Profiling of β-lactam selectivity for penicillin-binding proteins in
865 Escherichia coli strain DC2. *Antimicrobial agents and chemotherapy* **59**, 2785-2790 (2015).

866 61 Database resources of the National Center for Biotechnology Information. *Nucleic Acids Res* **44**,
867 D7-19, doi:10.1093/nar/gkv1290 (2016).

868 62 Darling, A. E., Jospin, G., Lowe, E., Matsen, F. A. t., Bik, H. M. & Eisen, J. A. PhyloSift:
869 phylogenetic analysis of genomes and metagenomes. *PeerJ* **2**, e243, doi:10.7717/peerj.243 (2014).

870 63 Ronquist, F., Teslenko, M., van der Mark, P., Ayres, D. L., Darling, A., Höhna, S., Larget, B., Liu,
871 L., Suchard, M. A. & Huelsenbeck, J. P. MrBayes 3.2: efficient Bayesian phylogenetic inference
872 and model choice across a large model space. *Syst Biol* **61**, 539-542, doi:10.1093/sysbio/sys029
873 (2012).

874 64 Letunic, I. & Bork, P. Interactive tree of life (iTOL) v3: an online tool for the display and annotation
875 of phylogenetic and other trees. *Nucleic acids research* **44**, W242-W245 (2016).

876 65 Lefort, V., Longueville, J.-E. & Gascuel, O. SMS: smart model selection in PhyML. *Molecular*
877 *biology and evolution* **6**, doi:10.1093/molbev/msx149 (2017).

878 66 Stamatakis, A. RAxML version 8: a tool for phylogenetic analysis and post-analysis of large
879 phylogenies. *Bioinformatics* **30**, 1312-1313, doi:10.1093/bioinformatics/btu033 (2014).

880 67 Seemann, T. Prokka: rapid prokaryotic genome annotation. *Bioinformatics* **30**, 2068-2069,
881 doi:10.1093/bioinformatics/btu153 (2014).

882 68 Cock, P. J. A., Antao, T., Chang, J. T., Chapman, B. A., Cox, C. J., Dalke, A., Friedberg, I.,
883 Hamelryck, T., Kauff, F., Wilczynski, B. & de Hoon, M. J. L. Biopython: freely available Python

884 tools for computational molecular biology and bioinformatics. *Bioinformatics* **25**, 1422-1423,
885 doi:10.1093/bioinformatics/btp163 (2009).

886 69 Shen, W., Le, S., Li, Y. & Hu, F. SeqKit: A Cross-Platform and Ultrafast Toolkit for FASTA/Q
887 File Manipulation. *PLOS ONE* **11**, e0163962, doi:10.1371/journal.pone.0163962 (2016).

888 70 Van Dongen, S. Graph Clustering Via a Discrete Uncoupling Process. *SIAM Journal on Matrix*
889 *Analysis and Applications* **30**, 121-141, doi:10.1137/040608635 (2008).

890 71 Sullivan, M. J., Petty, N. K. & Beatson, S. A. Easyfig: a genome comparison visualizer.
891 *Bioinformatics* **27**, 1009-1010, doi:10.1093/bioinformatics/btr039 (2011).

892 72 Deatherage, D. E. & Barrick, J. E. Identification of mutations in laboratory-evolved microbes from
893 next-generation sequencing data using breseq. *Methods Mol Biol* **1151**, 165-188, doi:10.1007/978-
894 1-4939-0554-6_12 (2014).

895 73 Letunic, I. & Bork, P. Interactive tree of life (iTOL) v3: an online tool for the display and annotation
896 of phylogenetic and other trees. *Nucleic Acids Res* **44**, W242-245, doi:10.1093/nar/gkw290 (2016).

897 74 Dion, M. F., Kapoor, M., Sun, Y., Wilson, S., Ryan, J., Vigouroux, A., van Teeffelen, S.,
898 Oldenbourg, R. & Garner, E. C. Bacillus subtilis cell diameter is determined by the opposing
899 actions of two distinct cell wall synthetic systems. *Nat Microbiol* **4**, 1294-1305,
900 doi:10.1038/s41564-019-0439-0 (2019).

901 75 Evinger, M. & Agabian, N. Envelope-associated nucleoid from Caulobacter crescentus stalked and
902 swarmer cells. *Journal of Bacteriology* **132**, 294-301 (1977).

903 76 Woldemeskel, S. A., McQuillen, R., Hessel, A. M., Xiao, J. & Goley, E. D. A conserved coiled-
904 coil protein pair focuses the cytokinetic Z-ring in Caulobacter crescentus. *Molecular microbiology*
905 **105**, 721-740 (2017).

906 77 West, L., Yang, D. & Stephens, C. Use of the Caulobacter crescentus genome sequence to develop
907 a method for systematic genetic mapping. *J Bacteriol* **184**, 2155-2166, doi:10.1128/jb.184.8.2155-
908 2166.2002 (2002).

909 78 Poindexter, J. L. S. & Cohen-Bazire, G. The fine structure of stalked bacteria belonging to the
910 family Caulobacteraceae. *The Journal of cell biology* **23**, 587-607 (1964).

911 79 Pate, J. L. & Ordal, E. J. The fine structure of two unusual stalked bacteria. *J Cell Biol* **27**, 133-
912 150, doi:10.1083/jcb.27.1.133 (1965).

913 80 Thanbichler, M., Iniesta, A. A. & Shapiro, L. A comprehensive set of plasmids for vanillate-and
914 xylose-inducible gene expression in Caulobacter crescentus. *Nucleic acids research* **35**, e137-e137
915 (2007).

916 81 Lu, H., Chen, L., Kong, L., Huang, L. & Chen, G. Asticcacaulis aquaticus sp. nov., Asticcacaulis
917 currens sp. nov. and Asticcacaulis machinosus sp. nov., isolated from streams in PR China. *Int J*
918 *Syst Evol Microbiol* **73**, doi:10.1099/ijsem.0.005974 (2023).

919 82 Vasilyeva, L. V., Omelchenko, M. V., Berestovskaya, Y. Y., Lysenko, A. M., Abraham, W. R.,
920 Dedysh, S. N. & Zavarzin, G. A. Asticcacaulis benevestitus sp. nov., a psychrotolerant, dimorphic,
921 prosthecate bacterium from tundra wetland soil. *Int J Syst Evol Microbiol* **56**, 2083-2088,
922 doi:10.1099/ijs.0.64122-0 (2006).

923 83 Staley, J. T., Bont, J. A. & Jonge, K. Prosthecobacter fusiformis nov. gen. et sp., the fusiform
924 caulobacter. *Antonie Van Leeuwenhoek* **42**, 333-342, doi:10.1007/bf00394132 (1976).

925 84 Quan, Z. X., Zeng, D. N., Xiao, Y. P., Roh, S. W., Nam, Y. D., Chang, H. W., Yoon, J. H., Oh, H.
926 M. & Bae, J. W. Henriciella marina gen. nov., sp. nov., a novel member of the family
927 Hyphomonadaceae isolated from the East Sea. *J Microbiol* **47**, 156-161, doi:10.1007/s12275-008-
928 0290-0 (2009).

929 85 Schlesner, H., Bartels, C., Sittig, M., Dorsch, M. & Stackebrandt, E. Taxonomic and phylogenetic
930 studies on a new taxon of budding, hyphal Proteobacteria, Hirschia baltica gen. nov., sp. nov. *Int J*
931 *Syst Bacteriol* **40**, 443-451, doi:10.1099/00207713-40-4-443 (1990).

932 86 URAKAMI, T., SASAKI, J., SUZUKI, K.-I. & KOMAGATA, K. Characterization and
933 Description of Hyphomicrobium denitrificans sp. nov. *International Journal of Systematic and*
934 *Evolutionary Microbiology* **45**, 528-532, doi:https://doi.org/10.1099/00207713-45-3-528 (1995).

935 87 Moore, R. L. The biology of Hyphomicrobium and other prosthecate, budding bacteria. *Annu Rev*
936 *Microbiol* **35**, 567-594, doi:10.1146/annurev.mi.35.100181.003031 (1981).

937 88 Hirsch, P. Budding bacteria. *Annu Rev Microbiol* **28**, 391-444,
938 doi:10.1146/annurev.mi.28.100174.002135 (1974).

939 89 Cserti, E., Rosskopf, S., Chang, Y. W., Eisheuer, S., Selter, L., Shi, J., Regh, C., Koert, U., Jensen,
940 G. J. & Thanbichler, M. Dynamics of the peptidoglycan biosynthetic machinery in the stalked
941 budding bacterium Hyphomonas neptunium. *Mol Microbiol* **103**, 875-895, doi:10.1111/mmi.13593
942 (2017).

943 90 Abraham, W. R., Strömpl, C., Meyer, H., Lindholst, S., Moore, E. R., Christ, R., Vancanneyt, M.,
944 Tindall, B. J., Bennasar, A., Smit, J. & Tesar, M. Phylogeny and polyphasic taxonomy of
945 Caulobacter species. Proposal of Maricaulis gen. nov. with Maricaulis maris (Poindexter) comb.
946 nov. as the type species, and emended description of the genera Brevundimonas and Caulobacter.
947 *Int J Syst Bacteriol* **49 Pt 3**, 1053-1073, doi:10.1099/00207713-49-3-1053 (1999).

948 91 Strömpl, C., Hold, G. L., Lünsdorf, H., Graham, J., Gallacher, S., Abraham, W. R., Moore, E. R.
949 & Timmis, K. N. Oceanicaulis alexandrii gen. nov., sp. nov., a novel stalked bacterium isolated
950 from a culture of the dinoflagellate Alexandrium tamarense (Lebour) Balech. *Int J Syst Evol*
951 *Microbiol* **53**, 1901-1906, doi:10.1099/ijs.0.02635-0 (2003).

952 92 Wu, N., Wu, Y., Liu, L., Zhang, Q., Lv, Y., Yuan, Y., He, J. & Shen, Q. Peiella sedimenti gen.
953 nov., sp. nov., a novel taxon within the family Caulobacteraceae isolated from sediment of a river.
954 *International Journal of Systematic and Evolutionary Microbiology* **74**,
955 doi:https://doi.org/10.1099/ijsem.0.006344 (2024).

956 93 Lee, K., Lee, H. K., Choi, T. H. & Cho, J. C. Robiginitomaculum antarcticum gen. nov., sp. nov.,
957 a member of the family Hyphomonadaceae, from Antarctic seawater. *Int J Syst Evol Microbiol* **57**,
958 2595-2599, doi:10.1099/ijs.0.65274-0 (2007).

959

Figure 1

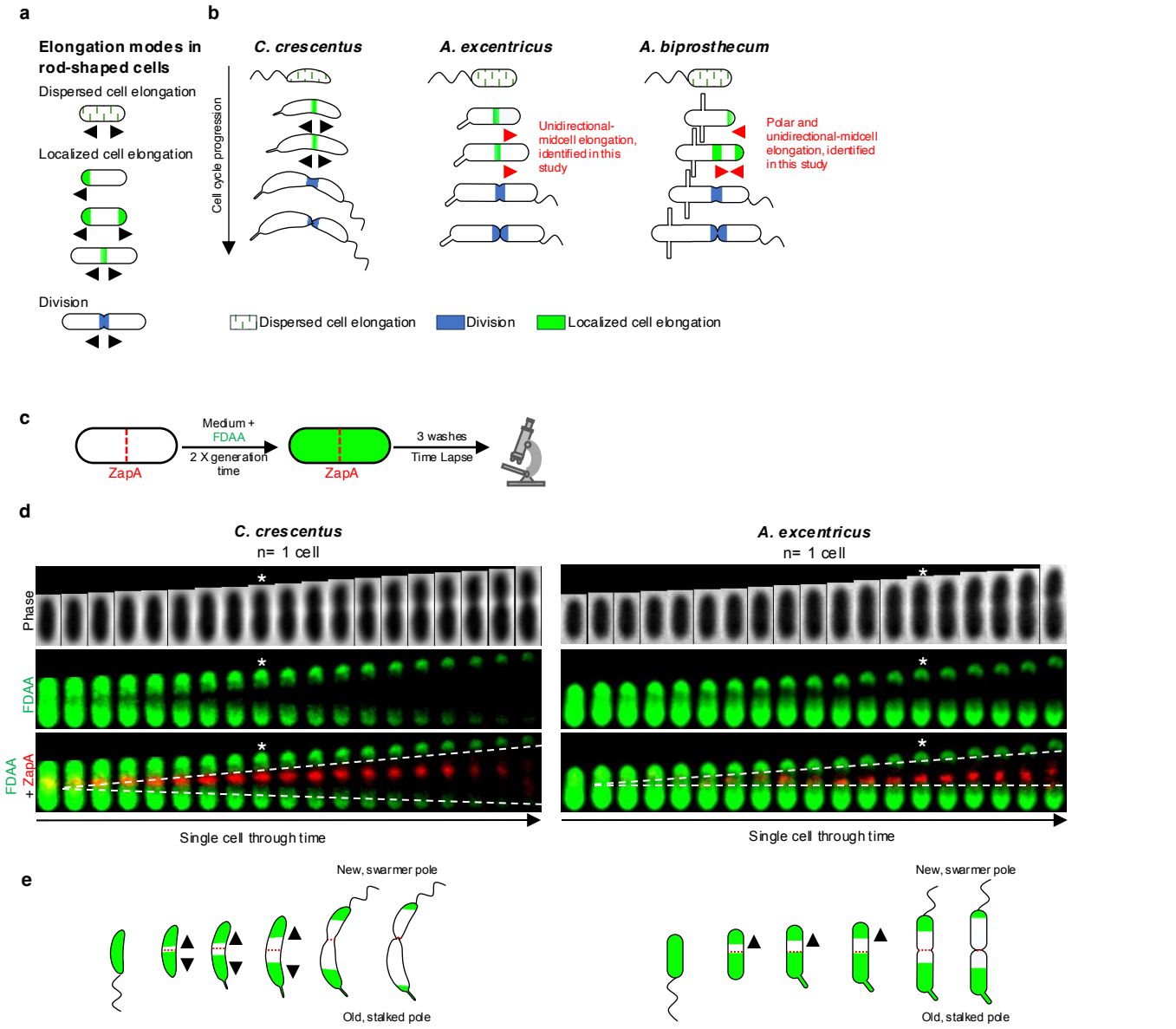
a
b
Elongation modes in rod-shaped cells
Dispersed cell elongation
Localized cell elongation
Division
C. crescentus
A. excentricus
A. biprosthecum
Cell cycle progression
Unidirectional-midcell elongation, identified in this study
Polar and unidirectional-midcell elongation, identified in this study
Dispersed cell elongation
Division
Localized cell elongation
c
ZapA
Medium + FDAA
2 X generation time
ZapA
3 washes
Time Lapse
d
C. crescentus
n= 1 cell
A. excentricus
n= 1 cell
Phase
FDAA
FDAA + ZapA
Single cell through time
Single cell through time
e
New, swarmer pole
Old, stalked pole
New, swarmer pole
Old, stalked pole

FIGURE LEGENDS

Fig. 1: Diversity of growth modes in rod-shaped bacteria and members of the *Caulobacteraceae* family.

(a) Schematic illustrating different growth modes observed among rod-shaped bacteria. Green lines represent lateral or dispersed elongation, solid green denotes different modes of localized cell elongation, and solid blue marks cell division.

(b) Dimorphic cell cycles and growth modes in *C. crescentus*, *A. excentricus* and *A. biprosthecum*. At the beginning of their cell cycle, *C. crescentus* swarmer cells elongate by dispersed insertion of new PG material (green lines) before bidirectional elongation near the midcell (green), followed by cell division (blue). In this study, we show that *A. excentricus* swarmer cells also undergo dispersed elongation (green lines) during the swarmer stage. However, this is followed by a novel, unidirectional-midcell elongation towards the new pole (green) prior to bidirectional cell division (blue). Finally, we identified that *A. biprosthecum* cells elongate through yet another novel mode of elongation – a combination of polar and unidirectional-midcell elongation.

(c) Schematic depicting the pulse-chase experiment using FDAA. Whole-cell PG was labeled with 500 µm FDAA (the "pulse," colored in green) over two generations, followed by washes with PYE to remove free FDAA from the medium. Subsequent growth in the absence of FDAA (the "chase") was observed using time-lapse microscopy. During the chase period, the loss of FDAA signal corresponds to new PG synthesis/turnover. The red dashed line indicates the position of the ZapA fluorescent protein fusion, as a marker of the future division site.

(**d**) Pulse-chase experiments using FDAAs in *C. crescentus* and *A. excentricus* cells carrying fluorescent fusions of the cell division protein ZapA. Images were taken every 5 minutes during the chase period. Kymographs show the loss of FDAA fluorescence as the cells grow. In *C. crescentus* (left), the FDAA BADA was used in combination with ZapA-mCherry. In *A. excentricus* (right), the FDAA TADA was used in combination with ZapA-sfGFP. Kymographs from both these species present the FDAA signal in green and the ZapA fluorescent fusion signal in red. White stars indicate cells starting division. See Extended Data Fig.1 for additional kymographs from each species.

(**e**) Schematic of FDAA signal loss in *C. crescentus* and *A. excentricus* cells. The red dashed line indicates the position of ZapA as a marker of the future division site. Green shading represents the old PG labeled with FDAA.

Figure 2

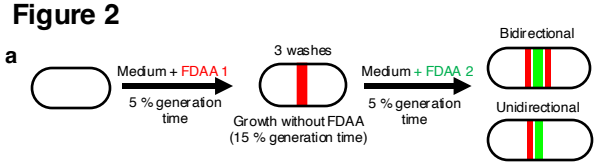
a
Medium + FDAA 1
5 % generation time
3 washes
Growth without FDAA
(15 % generation time)
Medium + FDAA 2
5 % generation time
Bidirectional
Unidirectional

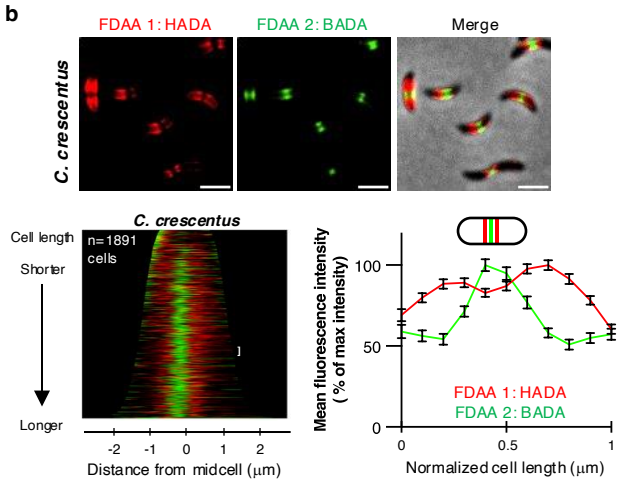
b
FDAA 1: HADA
FDAA 2: BADA
Merge
C. crescentus
C. crescentus
Cell length
Shorter
Longer
n=1891 cells
-2 -1 0 1 2
Distance from midcell (μm)
Mean fluorescence intensity (% of max intensity)
100
50
0
FDAA 1: HADA
FDAA 2: BADA
0 0.5 1
Normalized cell length (μm)

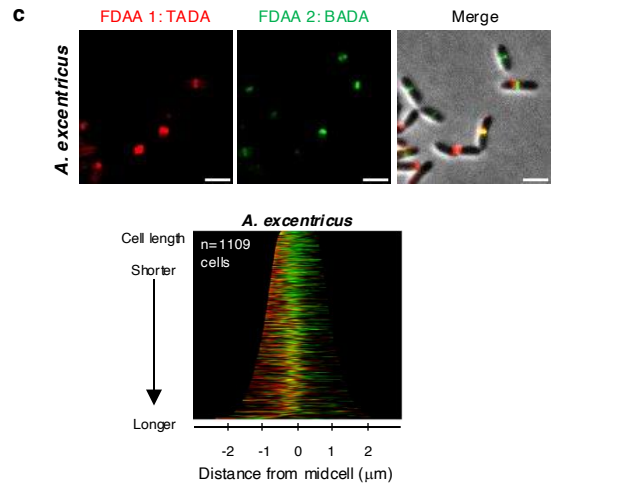
c
FDAA 1: TADA
FDAA 2: BADA
Merge
A. excentricus
A. excentricus
Cell length
Shorter
Longer
n=1109 cells
-2 -1 0 1 2
Distance from midcell (μm)

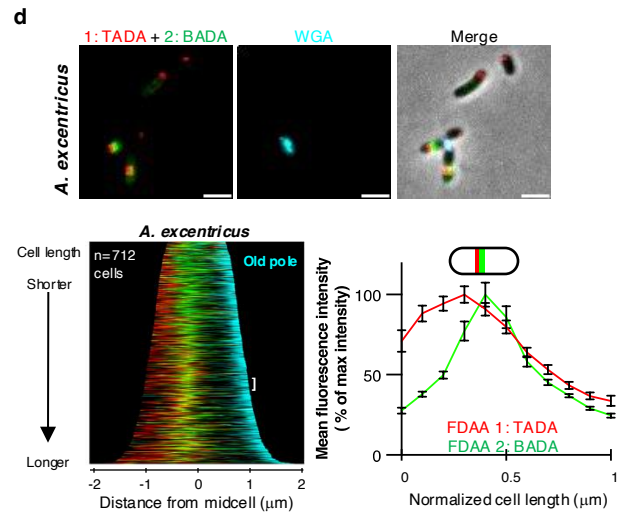
d
1: TADA + 2: BADA
WGA
Merge
A. excentricus
A. excentricus
Cell length
Shorter
Longer
n=712 cells
Old pole
-2 -1 0 1 2
Distance from midcell (μm)
Mean fluorescence intensity (% of max intensity)
100
50
0
FDAA 1: TADA
FDAA 2: BADA
0 0.5 1
Normalized cell length (μm)

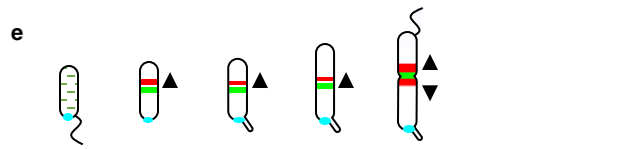
e
Labeling patterns at different stages of the cell cycle

Fig. 2. Sequential FDAA labeling reveals that *C. crescentus* grows bidirectionally from the midcell, while *A. excentricus* grows unidirectionally from the midcell towards the new pole.

(a) Schematic depicting the dual short-pulse experiment: sequential, dual short FDAA pulses show sites of active PG synthesis. Cells were first labeled with one FDAA (HADA in *C. crescentus* or TADA in *A. excentricus*, red) for 5% of their generation time, washed with PYE to remove the free FDAA, allowed to grow for 15 % of their generation time and then labeled with a second FDAA (green) for 5% of their generation time, washed again, and imaged with phase and fluorescence microscopy.

(b-d) Sequential FDAA labeling in *C. crescentus* (**b**) and *A. excentricus* (**c-d**). *Top*: Representative images are shown. Left to right: FDAA 1, FDAA 2 and merge images. Scale bars: 2 µm. *Middle*: population-level demographs showing the localization of the fluorescence intensities of FDAA 1 and FDAA 2. *Bottom*: fluorescence intensity plots showing the fluorescence signals from both FDAAs. In Panel **d**, the old pole in *A. excentricus* cells is additionally labeled with fluorescent WGA (cyan). In all demographs, cells are arranged by length, with 50% of maximum fluorescence intensities shown. Demographs in Panels **b-c** are oriented with the maximum fluorescence intensity of the second FDAA to the left, and in Panel **d** with the WGA-labeled old pole (cyan) to the right. In Panels **b** and **d**, the white brackets show the 50 cells selected to plot the fluorescence intensities of the two FDAAs along the cell length, shown in the graphs adjacent to the demographs. To generate these graphs, points were selected along the medial axis of each cell, and the normalized signals of FDAA 1 (red) and FDAA 2 (green) were plotted relative to their normalized position along the cell length. The lines represent the mean values, with error bars showing the standard error of the mean (SEM).
See Extended Data Fig. 2 for additional demographs showing each FDAA individually, and at 50% and 100% fluorescence intensities.

(**e**) Schematic illustrating PG synthesis at different stages of the *A. excentricus* cell cycle. Smaller swarmer cells undergo dispersed cell elongation (green dots). As they differentiate into stalked cells, they elongate unidirectionally from the midcell towards the new cell pole, with the first FDAA signal (red) located on the new pole side of the second FDAA signal (green). Predivisional cells or cells undergoing septation exhibit bidirectional growth at the midcell, with red signals on both sides of the second FDAA signal (green). The old pole is indicated by the holdfast (cyan).

Figure 3

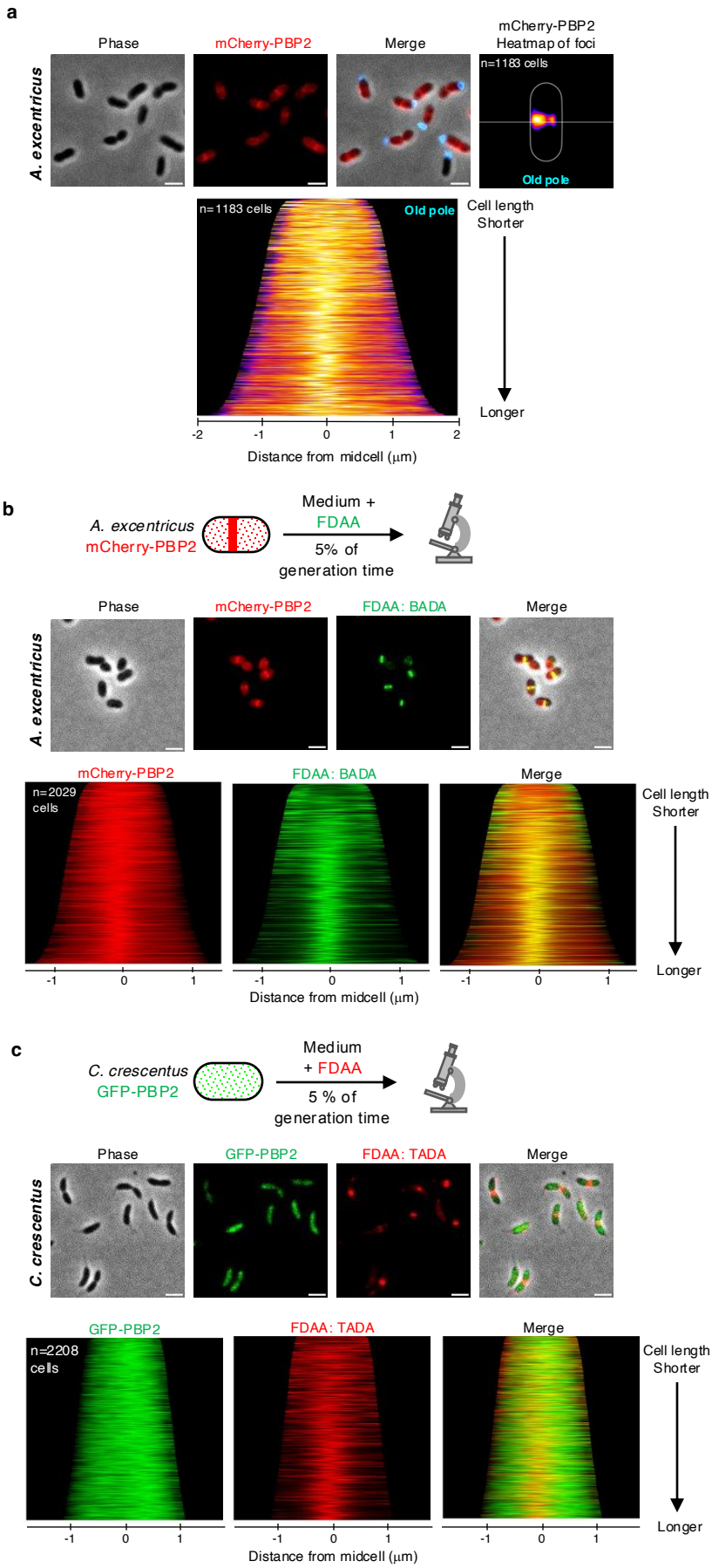
a
Phase
mCherry-PBP2
Merge
mCherry-PBP2
Heatmap of foci
A. excentricus
n=1183 cells
Old pole
n=1183 cells
Old pole
Cell length
Shorter
Longer
-2
-1
0
1
2
Distance from midcell (μm)
b
A. excentricus
mCherry-PBP2
Medium +
FDAA
5% of
generation time
Phase
mCherry-PBP2
FDAA: BADA
Merge
A. excentricus
mCherry-PBP2
FDAA: BADA
Merge
n=2029
cells
Cell length
Shorter
Longer
-1
0
1
Distance from midcell (μm)
c
C. crescentus
GFP-PBP2
Medium
+ FDAA
5 % of
generation time
Phase
GFP-PBP2
FDAA: TADA
Merge
C. crescentus
GFP-PBP2
FDAA: TADA
Merge
n=2208
cells
Cell length
Shorter
Longer
-1
0
1
Distance from midcell (μm)

Fig 3. Distinct PBP2 localization in *A. excentricus* and *C. crescentus* and its correlation with active PG synthesis.

(a) Subcellular localization of mCherry-PBP2 in *A. excentricus*. *Top:* Representative images are shown. Left to right: Phase, mCherry-PBP2 fluorescence and merged images. Scale bar: 2 μm. A heatmap of mCherry-PBP2 foci at the population level is displayed. In the heatmap, cells were oriented using the old pole labeled with WGA (cyan), with the white line indicating the midcell. *Bottom*: A demograph showing the localization of mCherry-PBP2 fluorescence at the population level, with cells arranged by length and oriented with the old pole towards the right.

(b) Short-pulse FDAA (BADA) labeling of the *A. excentricus* mCherry-PBP2 strain. *Top:* A schematic depicting the experiment. Cells were labeled with 250 μM BADA for 5% of their generation time, fixed with 70% (v/v) ethanol and imaged. *Middle:* Representative phase, fluorescence (mCherry-PBP2 and BADA) and merged images are shown. Scale bar: 2 μm. *Bottom:* Population-level demographs showing the localization of the fluorescence intensities of mCherry-PBP2, BADA and their overlays. See Extended Data Fig. 4a for heatmaps and density maps of mCherry-PBP2 and BADA at the population level.

(c) Short-pulse FDAA (TADA) labeling of the *C. crescentus* GFP-PBP2 strain. *Top:* A schematic depicting the experiment. Cells were labeled with 250 μM TADA for 5% of their generation time, fixed with 70% (v/v) ethanol and imaged. *Middle:* Representative phase, fluorescence (GFP-PBP2 and TADA) and merged images are shown. Scale bar: 2 μm. *Bottom:* Population-level demographs showing the localization of the fluorescence intensities of GFP-PBP2, TADA and their overlays.

See Extended Data Fig. 4b-c for additional fluorescence images and population-level demographs showing the differences in localization of PBP2 in *A. excentricus* vs. *C. crescentus*.

Figure 4

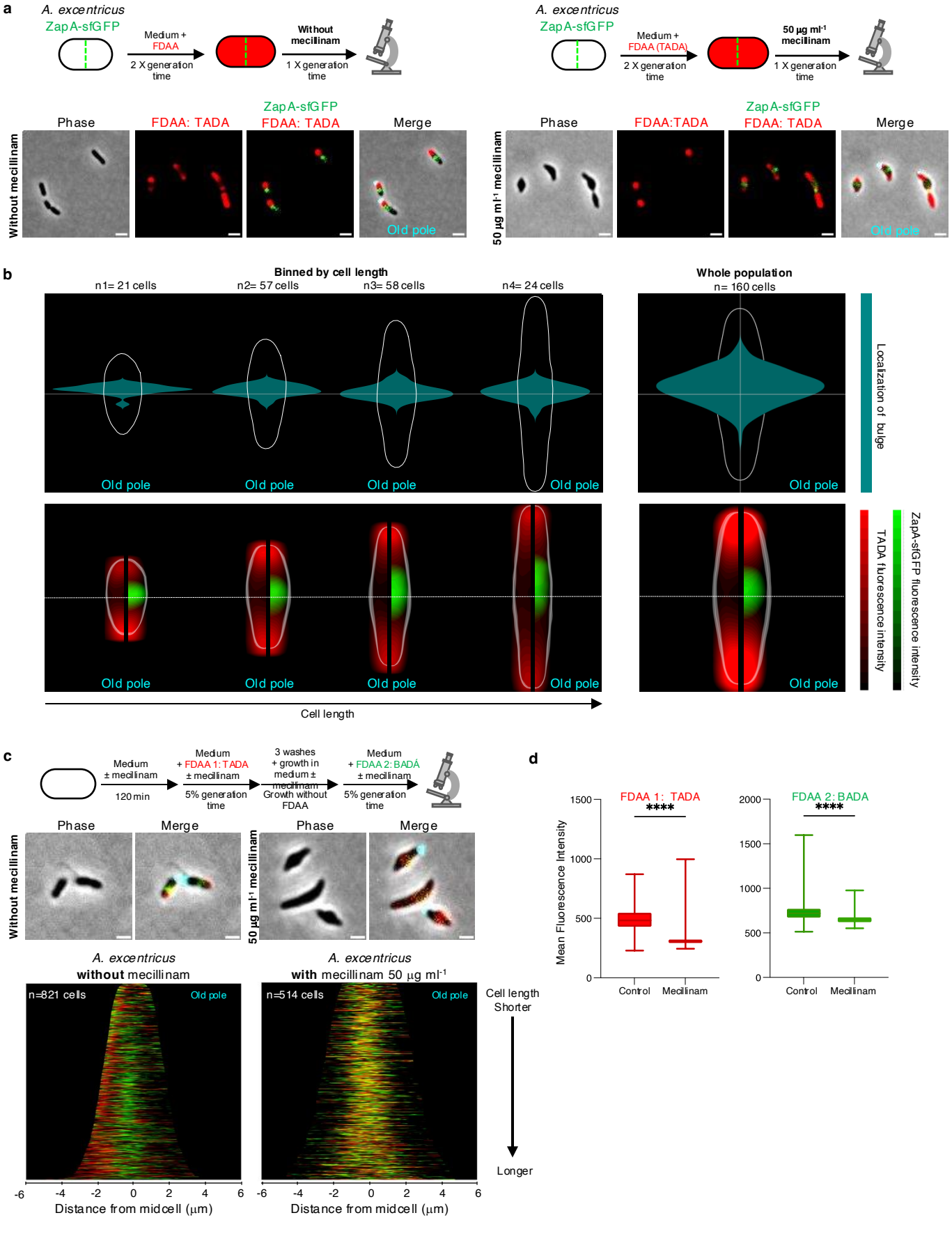
a
A. excentricus
ZapA-sfGFP
Medium + FDAA
2 X generation time
Without mecillinam
1 X generation time
A. excentricus
ZapA-sfGFP
Medium + FDAA (TADA)
2 X generation time
50 µg ml-1 mecillinam
1 X generation time
Phase
FDAA: TADA
ZapA-sfGFP FDAA: TADA
Merge
Without mecillinam
Old pole
Phase
FDAA:TADA
ZapA-sfGFP FDAA: TADA
Merge
50 µg ml-1 mecillinam
Old pole
b
Binned by cell length
n1= 21 cells
n2= 57 cells
n3= 58 cells
n4= 24 cells
Whole population
n= 160 cells
Old pole
Localization of bulge
TADA fluorescence intensity
ZapA-sfGFP fluorescence intensity
Cell length
c
Medium ± mecillinam
120 min
Medium + FDAA 1: TADA ± mecillinam
5% generation time
3 washes + growth in medium ± mecillinam
Growth without FDAA
Medium + FDAA 2: BADA ± mecillinam
5% generation time
Phase
Merge
Without mecillinam
50 µg ml-1 mecillinam
A. excentricus without mecillinam
A. excentricus with mecillinam 50 µg ml-1
n=821 cells
n=514 cells
Old pole
Cell length
Shorter
Longer
-6 -4 -2 0 2 4 6
Distance from midcell (µm)
d
FDAA 1: TADA
FDAA 2: BADA
****
Mean Fluorescence Intensity
0
500
1000
1500
2000
Control
Mecillinam

Fig 4. PBP2 is responsible for unidirectional PG synthesis at the midcell in *A. excentricus*

(**a**) *Top:* Schematic depicting pulse-chase experiments in *A. excentricus* ZapA-sfGFP cells with (*right*) or without (*left*) mecillinam treatment. Whole-cell PG was labeled with TADA (red) over two generations, followed by washing and growth with or without mecillinam (50 μg ml^{-1}) over one generation before imaging. *Bottom:* Representative phase, fluorescence and merged images from both conditions are shown. The fluorescence images show TADA individually as well as overlaid with ZapA-sfGFP. The merged image shows phase overlaid with TADA, ZapA-sfGFP and WGA fluorescence. Scale bar: 2 μm.

(**b**) ShapePlots of *A. excentricus* cells after an FDAA pulse-chase experiment, with mecillinam treatment during the chase period. *Top:* Shape plots showing bulge localization. *Bottom:* ShapePlots show ZapA-sfGFP and FDAA signal loss following the chase period. Each ShapePlot is divided longitudinally (black line) to show the loss of FDAA signal exclusively on the left, and overlaid with ZapA-sfGFP on the right.
ShapePlots are presented individually for four categories of cells binned by cell length (*left*) as well as for the entire population of 160 cells (*right*). All cells are oriented using WGA-labeling of the holdfast, positioning the old pole at the bottom. Horizontal white lines represent the midcell.

(c) *Top:* Schematic of a dual short-pulse experiment with or without mecillinam (50 μg ml^{-1}) to show active PG synthesis. *A. excentricus* cells were first allowed to grow over 120 min with or without mecillinam. Cells were then labeled with TADA (red) for 5% of their generation time, washed to remove excess FDAA, allowed to grow for 18 min, and then labeled with BADA (green) for 5% of their generation time, with or without mecillinam. They were then washed again and imaged with phase and fluorescence microscopy. *Middle:* Representative phase and merged images from both treatment conditions – with and without mecillinam. Merged images show phase contrast overlaid with fluorescence signals from the two FDAAs as well as WGA-labeled holdfast (cyan). Scale bar: 2 μm. Look up tables (LUTs) were adjusted for each condition to have a visible FDAA signal, and therefore were not identical. *Bottom:* Population-level demographs showing the fluorescence intensities of both FDAA signals, with and without mecillinam treatment. Cells were arranged by length, with the old pole to the right. 50% of the maximum fluorescence intensities are shown.

(**d**) Box graphs showing quantification of fluorescence intensities for each FDAA pulse in the presence or absence of mecillinam (for the same cells quantified in the demographs in 4c). **** $P<0.0001$ (Welch One-Way ANOVA Test). Error bars show the standard error of the mean (SEM).

Figure 5

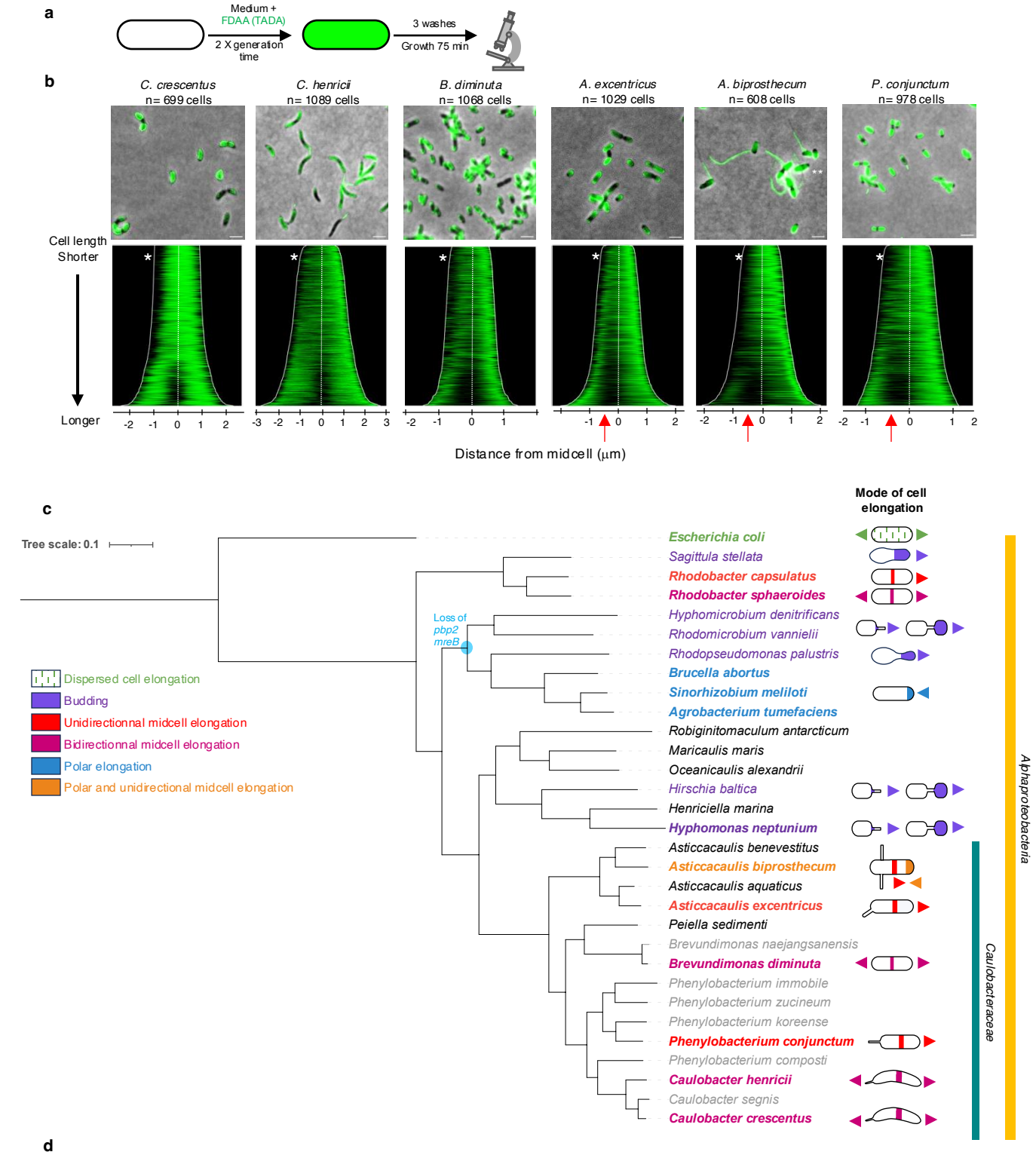
a
Medium + FDAA (TADA)
2 X generation time
3 washes
Growth 75 min
b
C. crescentus n= 699 cells
C. henricii n= 1089 cells
B. diminuta n= 1068 cells
A. excentricus n= 1029 cells
A. biprosthecum n= 608 cells
P. conjunctum n= 978 cells
Cell length
Shorter
Longer
Distance from midcell (μm)
c
Mode of cell elongation
Tree scale: 0.1
Loss of pbp2 mreB
Dispersed cell elongation
Budding
Unidirectionnal midcell elongation
Bidirectionnal midcell elongation
Polar elongation
Polar and unidirectional midcell elongation
Escherichia coli
Sagittula stellata
Rhodobacter capsulatus
Rhodobacter sphaeroides
Hyphomicrobium denitrificans
Rhodomicrobium vannielii
Rhodopseudomonas palustris
Brucella abortus
Sinorhizobium meliloti
Agrobacterium tumefaciens
Robiginitomaculum antarcticum
Maricaulis maris
Oceanicaulis alexandrii
Hirschia baltica
Henriciella marina
Hyphomonas neptunium
Asticcacaulis benevestitus
Asticcacaulis biprosthecum
Asticcacaulis aquaticus
Asticcacaulis excentricus
Peiella sedimenti
Brevundimonas naejangsanensis
Brevundimonas diminuta
Phenylobacterium immobile
Phenylobacterium zucineum
Phenylobacterium koreense
Phenylobacterium conjunctum
Phenylobacterium composti
Caulobacter henricii
Caulobacter segnis
Caulobacter crescentus
Alphaproteobacteria
Caulobacteraceae
d
Scenarios for ancestral mode of cell elongation:
Unidirectional midcell elongation
A. excentricus
B. diminuta
P. conjunctum
C. crescentus
Bidirectional midcell elongation
A. excentricus
B. diminuta
P. conjunctum
C. crescentus

Fig. 5. Diversity of cell elongation modes in members of the *Caulobacteraceae* family

(a) Schematic depicting the pulse-chase experiment using FDAAs. Whole-cell PG was labeled with TADA for two generations, washed to remove excess FDAA, followed by a chase period of 75 minutes before imaging.

(b) Demograph analysis of pulse-chase experiments in WT cells of *C. crescentus*, *C. henricii*, *P. conjunctum*, *B. diminuta*, *A. excentricus*, and *A. biprosthecum*. Loss of FDAA labeling shows sites of PG synthesis/remodeling. Cells are arranged by length, with each cell oriented so that the pole with the maximum fluorescence intensity is to the right. White stars indicate signal loss at one pole. Red arrows highlight unidirectional midcell elongation in *A. excentricus*, *A. biprosthecum*, and *P. conjunctum,* as observed by greater FDAA signal loss towards the left of the demograph.

(c) Phylogenetic tree of representative species from the Alphaproteobacteria*,* which includes the family *Caulobacteraceae.* Taxon label colors correspond to different modes of cell elongation: dispersed cell elongation (green), unidirectional midcell elongation (red), polar elongation (blue), budding (violet), polar and unidirectional midcell elongation (orange and red), bidirectional midcell elongation (magenta), binary fission (black), and unknown (grey). Species for which the cell elongation mode has been studied using FDAAs, TRSE or other methods are highlighted in bold. The node where *pbp2* and *mreB* (and the associated *mreCD* and *rodA* genes) are predicted to have been lost within the *Rhizobiales* is highlighted in blue. The tree, based on a concatenation conserved protein-coding gene sequences, is fully supported, with posterior probabilities of 1 for all clades. See the online Methods section for details on phylogenetic reconstruction and refer to **Table S3** for genome IDs and mode of cell elongation.

(d) This schematic, derived from a pruned version of the phylogenetic tree in Fig. 5a to highlight the species of interest, illustrates the identified modes of cell elongation and the possible number of transitions. The transitions are depicted assuming two scenarios: unidirectional cell elongation as the ancestral state (*left, red*) or bidirectional midcell elongation as the ancestral state (*right, magenta*). Colored lines and arrows (*red or magenta*) indicate where the transitions might have occurred.

Figure 6

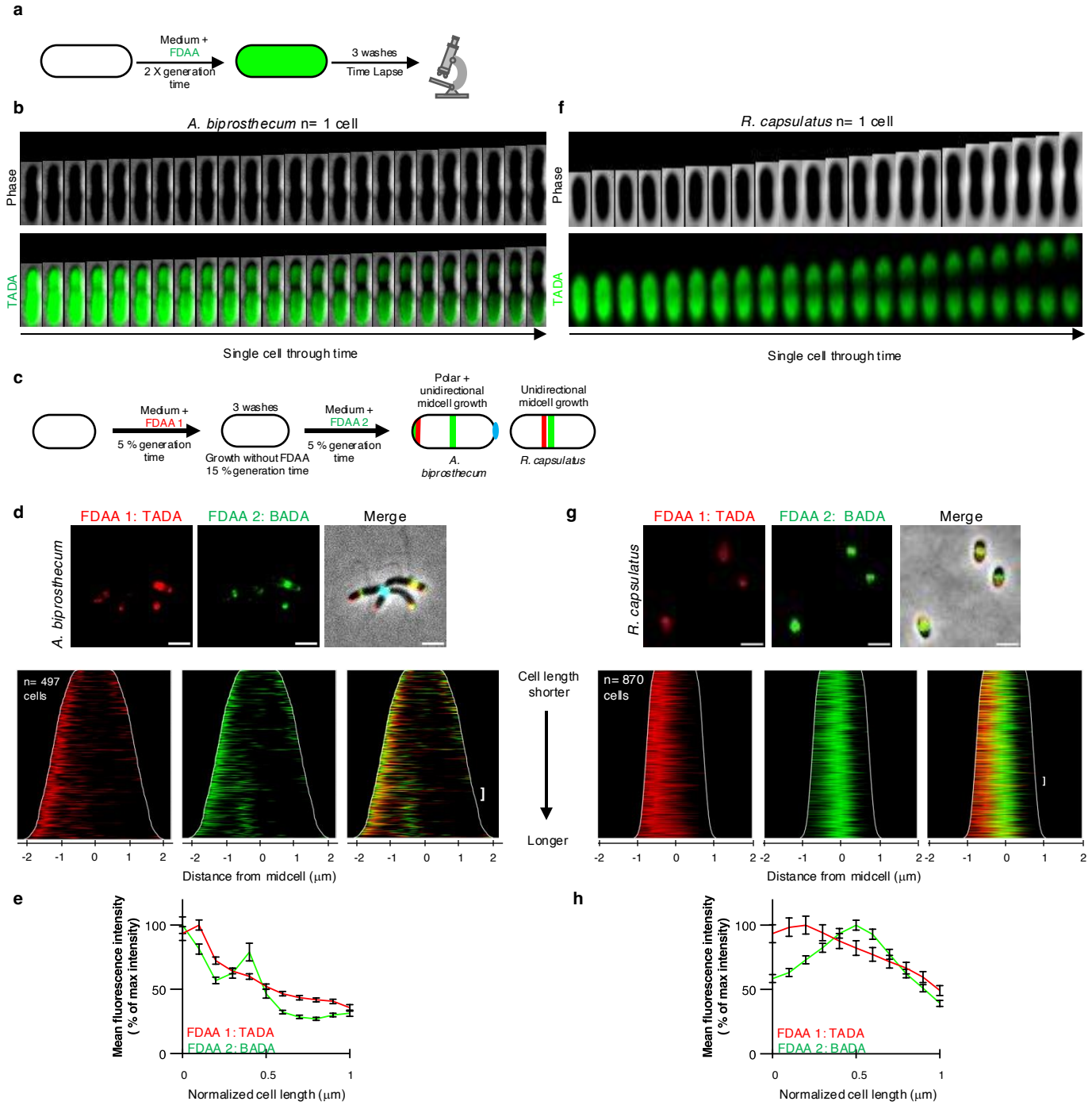
a
Medium + FDAA
2 X generation time
3 washes
Time Lapse
b
A. biprosthecum n= 1 cell
Phase
TADA
Single cell through time
f
R. capsulatus n= 1 cell
Phase
TADA
Single cell through time
c
Medium + FDAA 1
5 % generation time
3 washes
Growth without FDAA
15 % generation time
Medium + FDAA 2
5 % generation time
Polar + unidirectional midcell growth
Unidirectional midcell growth
A. biprosthecum
R. capsulatus
d
FDAA 1: TADA
FDAA 2: BADA
Merge
A. biprosthecum
n= 497 cells
Distance from midcell (μm)
Cell length shorter
Longer
g
FDAA 1: TADA
FDAA 2: BADA
Merge
R. capsulatus
n= 870 cells
Distance from midcell (μm)
e
Mean fluorescence intensity (% of max intensity)
FDAA 1: TADA
FDAA 2: BADA
Normalized cell length (μm)
h
Mean fluorescence intensity (% of max intensity)
FDAA 1: TADA
FDAA 2: BADA
Normalized cell length (μm)

Fig. 6. FDAA labeling experiments demonstrate polar and unidirectional midcell elongation in *A. biprosthecum* and unidirectional midcell elongation in *R. capsulatus*.

(a) Schematic depicting the FDAA pulse-chase experiments in *A. biprosthecum* and *R. capsulatus*. Whole-cell PG was labeled with 500 µm TADA (green) over two generations, followed by washes with medium to remove free FDAA from the medium. Subsequent growth in the absence of the FDAA (the chase) was followed by time-lapse microscopy. Loss of FDAA signal during the chase period corresponds to new PG synthesis/turnover.

(b,f) Kymographs of the pulse chase experiments showing the loss of FDAA fluorescence during the chase period in (**b**) *A. biprosthecum* and (**f**) *R. capsulatus*. Images were taken every 5 minutes. See Extended Data Fig. 6 and 7 for additional kymographs.

(c) Schematic depicting the dual short-pulse experiment showing active PG synthesis. Cells were first labeled with TADA for 5% of their generation time, washed with fresh media to remove free FDAA, allowed to grow without FDAA and then labeled with BADA for 5% of their generation time. Cells were then washed again and imaged with phase and fluorescence microscopy.

(d,g) Representative images and demographs showing the fluorescence intensity of both FDAA signals in **(d)** *A. biprosthecum* and **(g)** *R. capsulatus*. In the demographs, cells were arranged by length, with the old pole (labelled with WGA, not shown) to the right in *A. biprosthecum*, and with the maximum fluorescence intensity of the first FDAA to the left in *R. capsulatus*. 50% of the maximum fluorescence intensities are shown. The white brackets indicate the 50 cells selected to show the fluorescence profiles of the two FDAAs in (**e**) and (**f**). Scale bars: 2 µm. See Extended Data Fig. 6 and 7 for demographs showing each FDAA individually and with the full range of fluorescence signal.

(e,h) Fluorescence intensity profiles of FDAA 1 (TADA, red line) and FDAA 2 (BADA, green line) in (**e**) *A. biprosthecum* cells and (**h**) *R. capsulatus* cells, plotted from n = 50 cells for both species. Points were selected along the medial axis of each cell, and the normalized signal was plotted relative to position along the cell length. The lines represent the mean values, with error bars showing the standard error of the mean (SEM).